ANL/RAS 76-29

CONF-760622--55

F2 PHENOMENOLOGICAL TEST ON FUEL MOTION

(INTERIM REPORT)

by

R. G. Pal, C. L. Fink, R. R. Stewart,

S. M. Gehl and A. B. Rothman

September, 1976

*Contents of this report were presented at the Annual Meeting of the American Nuclear Society in Toronto, June, 1976.

Reactor Analysis and Safety Division
ARGONNE NATIONAL LABORATORY
9700 South Cass Avenue
Argonne, Illinois 60439

ANL/RAS 76-29

F2 PHENOMENOLOGICAL TEST ON FUEL MOTION

(INTERIM REPORT)

by

R. G. Palm, C. L. Fink, R. R. Stewart,

S. M. Gehl and A. B. Rothman

September, 1976

*Contents of this report were presented at the Annual Meeting of the American Nuclear Society in Toronto, June, 1976.

NOTICE: This informal document contains preliminary information prepared primarily for interim use in fast breeder reactor programs in the U.S. Since it does not constitute a final report, it should be cited as a reference only in special circumstances, such as requirements for regulatory needs.

Reactor Analysis and Safety Division
ARGONNE NATIONAL LABORATORY
9700 South Cass Avenue
Argonne, Illinois 60439

TABLE OF CONTENTS

LIST OF FIGURES

LIST OF TABLES

1.0 SUMMARY

TREAT F-series tests are being conducted to provide data on fuel motion at accident power levels from one to about ten times design for use in development of fuel motion models. Test F2 was conducted to evaluate motion of high power fuel in a hypothetical LMFBR unprotected TUC (transient undercooling) accident. Fuel, and fuel-boundary conditions following coolant boiling, and dryout under TUC conditions are achieved in each F-series test with a single fuel element surrounded by a nuclear heated wall in a dry test capsule. Test F2 was conducted with a low burnup but restructured fuel element to investigate the effect of fuel vapor pressure on fuel motion. Prior irradiation of the F2 fuel element in EBR-II was at 380 w/cm (11.6 kW/ft) to a burnup of 0.35 a/o. The F2 TREAT power transient had a 6.5 s constant power heatup internal generating 410 w/cm (12.5 kW/ft) of peak fuel linear power followed by a power burst to a level ~11 times the TREAT heatup power.

The hodoscope and heat transfer calculations indicated respectively that the fuel column was erect and not yet molten at the power burst initiation. In addition, burnout of the lower thermocouple indicated that significant molten clad drainage had occurred just before the power burst began (~10.5 s since transient initiation). Two major upward fuel movements occurred in the power burst during the period of rising TREAT power at ten times of 11.04 s and 11.18 s. The first dispersal moved molten fuel into a cool annular region above the original fuel column where the fuel froze almost immediately (within ~100 ms). At some unknown time during the power burst the heated wall partially melted and radially deformed. 17 ± 5 gms of dispersed material was found in the region above the original fuel column. Most of the dispersed material is test fuel rather than heated wall. The dispersed fuel is concentrated in a 10 cm long annular slug although fragments of fuel are found above the slug.

Final fuel arrangement also shows a region of ~20 cm in the upper part of the original fuel column region mostly voided of fuel with regions of dispersed fuel above and below the voided region. No unambiguous indication of what vapor species drove the fuel dispersal has been found, although fuel vapor is a strong candidate based upon the current analysis. Other candidate vapor species are fission products and stainless steel clad.

2.0 HARDWARE DESCRIPTION

The test vehicle for the F-series tests is a modified Mark-II loop body illustrated in Fig. 1. A single test fuel pin is in a sealed capsule which is located at one end of the test train. The test train is inserted into the loop from the top and sealed to the loop at the test train flange. Fig. 1 shows that the 34.3 cm (13.5 in.) long test fuel column is approximately centered in the 122 cm (48 in.) high TREAT core. A B_6Si thermal-neutron filter equivalent to .0456 cm (18 mils) thickness covers the outside of the loop body as illustrated. The purpose of the filter is to harden the TREAT neutron spectrum sufficiently to achieve the desired progression of melting in the cladding and fuel, prior to their motion in the test assembly. Dysprosium flux shaping collars were installed on the outside of the neutron filters in order to shape the test fuel axial power profile to that of EBR-II, the prior source of irradiation of the F-series fuel pins. When the Mark-II loop body is used for tests having flowing sodium, an electromagnetic pump is placed between the upper and lower bends. In the F-series, these bends were flanged off as indicated in Fig. 1. A burst disc was incorporated in the F-series loop to vent the loop to the dump tank if high loop pressure were to develop. Fig. 2 is an axial view of the F-series capsule located inside the Mark-II loop. Reference between Figs. 1 and 2 may be made by locating the upper bend of the Mark-II loop and the fuel column in each illustration. Fig. 2 was made to scale axially but not radially. The test fuel pin is located at the radial center of the sealed capsule. Axial motion of the fuel pin is constrained by a tungsten pin through the lower fuel pin end plug, and a fuel pin retainer on the top end plug. Note that the fuel pin retainer restricts downward but not upward movement of the top end plug. The fuel pin is surrounded radially by a W-UO_2 cermet (nuclear heated wall), a thin molybdenum reflector, a stainless

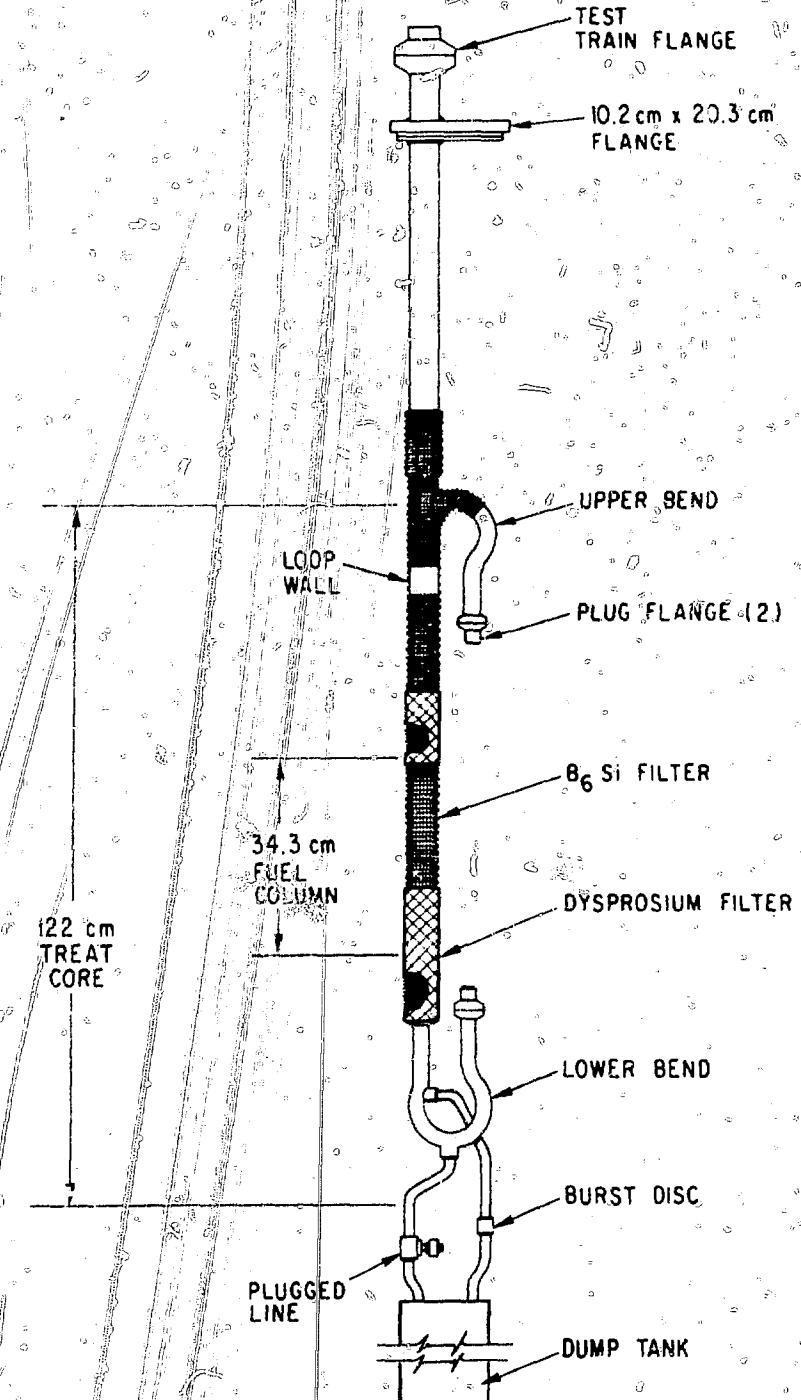

Fig. 1 F-Series Mark-II Loop

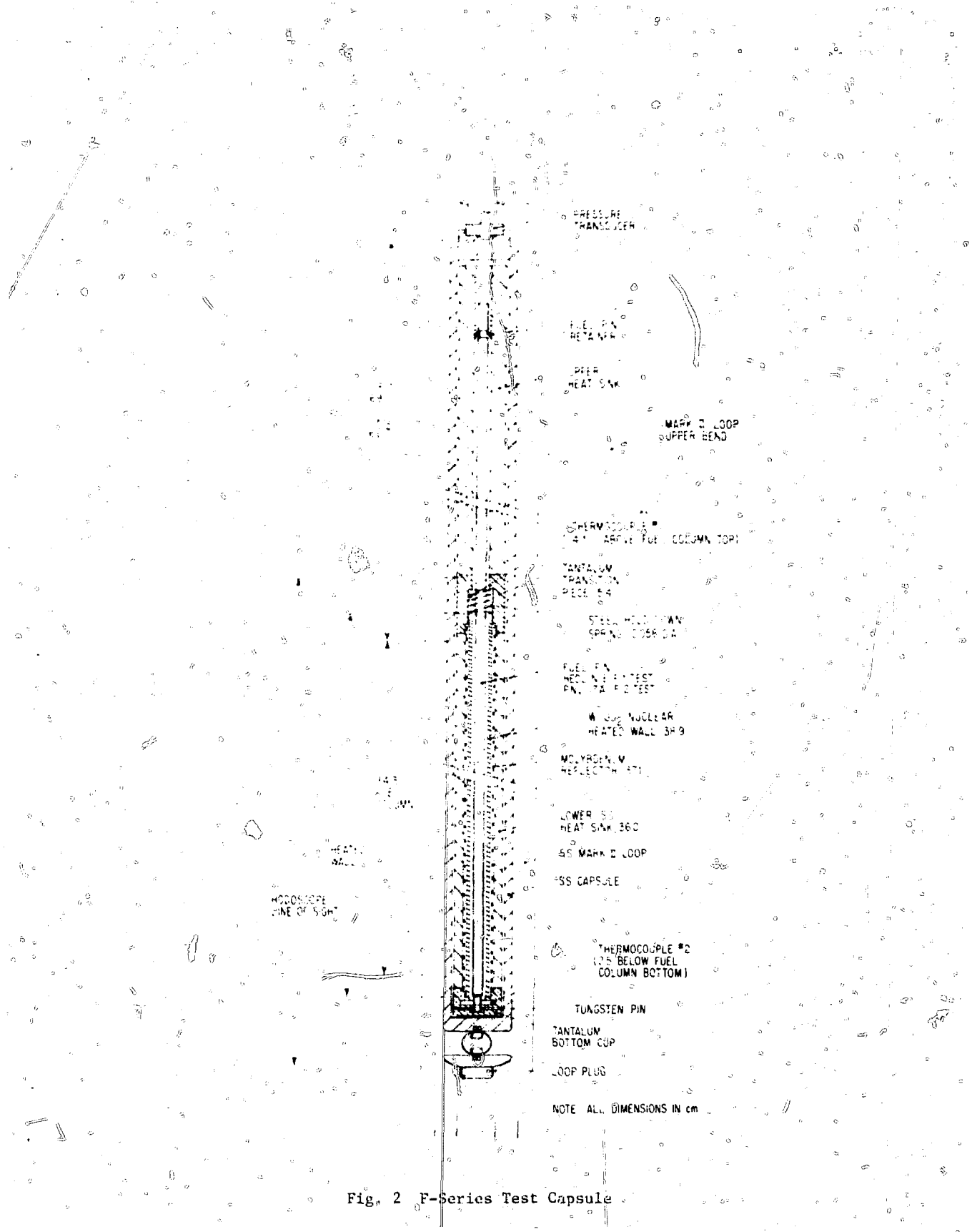

Fig. 2 F-Series Test Capsule

steel heat sink, and a stainless steel capsule wall. A scaled radial cross-section with dimensions of the F-series capsule and loop in the fueled region is shown in Fig. 3. Fig. 2 indicates that the heated wall extends 2.54 cm (1 in.) above the top of the fuel column and 2.06 cm (13/16 in.) below the fuel column for a total length of 38.9 cm (15 5/16 in). Two large tantalum pieces are located just beyond the ends of the fuel column. These pieces contain and align the heated wall; and in addition, the lower piece serves as a fuel catcher. Thermocouples 1 and 2 are located as shown just above and below the fuel column, respectively. These are stainless steel sheathed, Chromel-Alumel thermocouples. The capsule was filled with Ar-3% He to an absolute pressure of 83.4 kPa (12.1 psi) before the test. The pressure transducer (CEC model A-316 unbonded strain gauge type, ±689 kPa (±100 psi) linear range) is located at the top of the capsule. Fig. 1 shows that the distance from the top of the fuel column to the pressure transducer diaphragm is 67.2 cm (24.7 in.) in the F2 test. The fast-neutron hodoscope line of sight is also shown in Fig. 2. Fuel motion is continuously monitored by the fast-neutron hodoscope which was the principal test instrument for the F-series. Fig. 4 shows the F2 test pin. The pin was modified to fit into the F-series test capsule by shortening the bottom end plug and drilling a hole through it for the tungsten locking pin. Note also that the spiral wire wrap was removed from the fuel pin. Table I summarizes data on the F2 fuel pin.

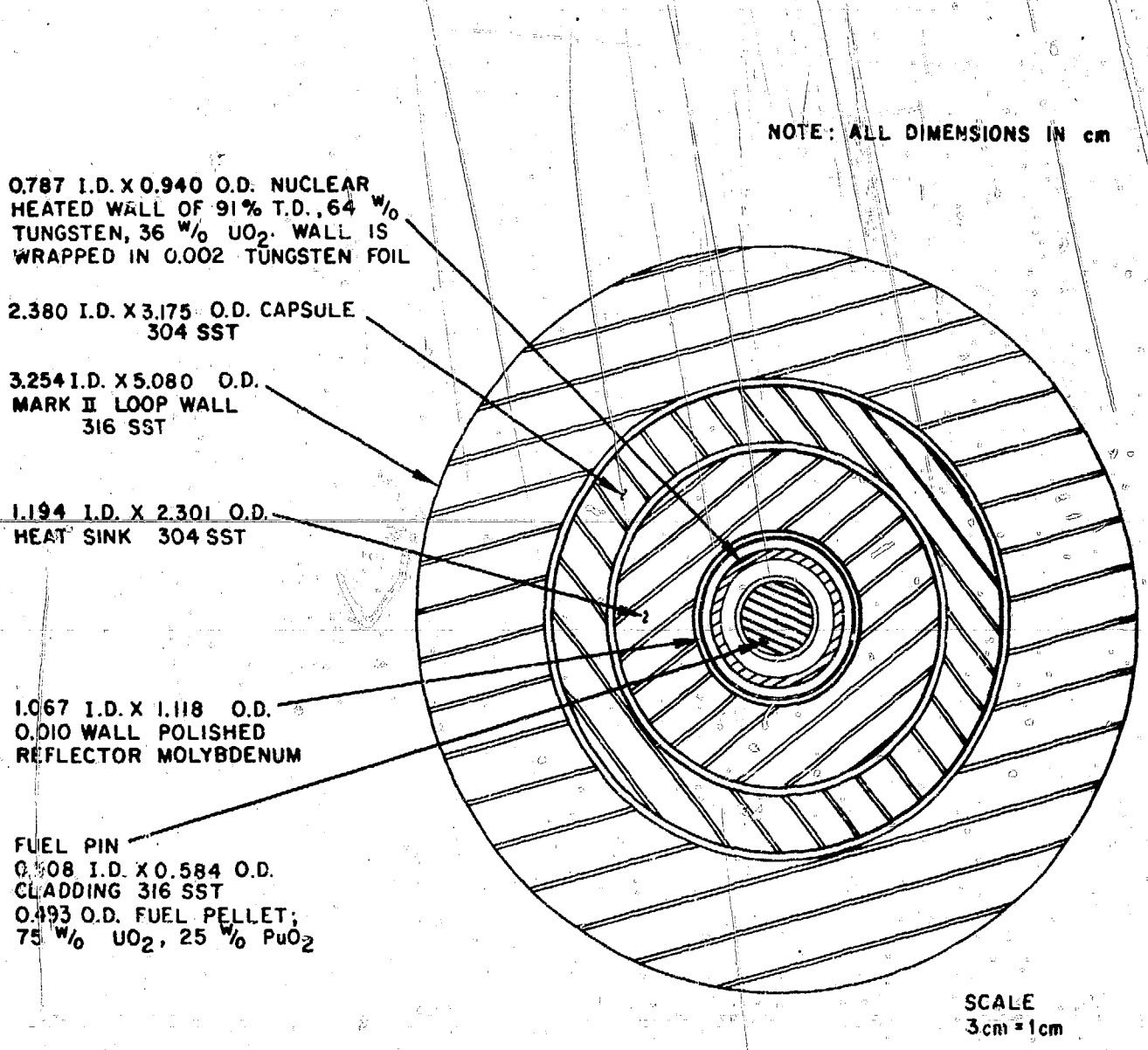

Fig. 3 F-Series Cross Section Through Test Fuel

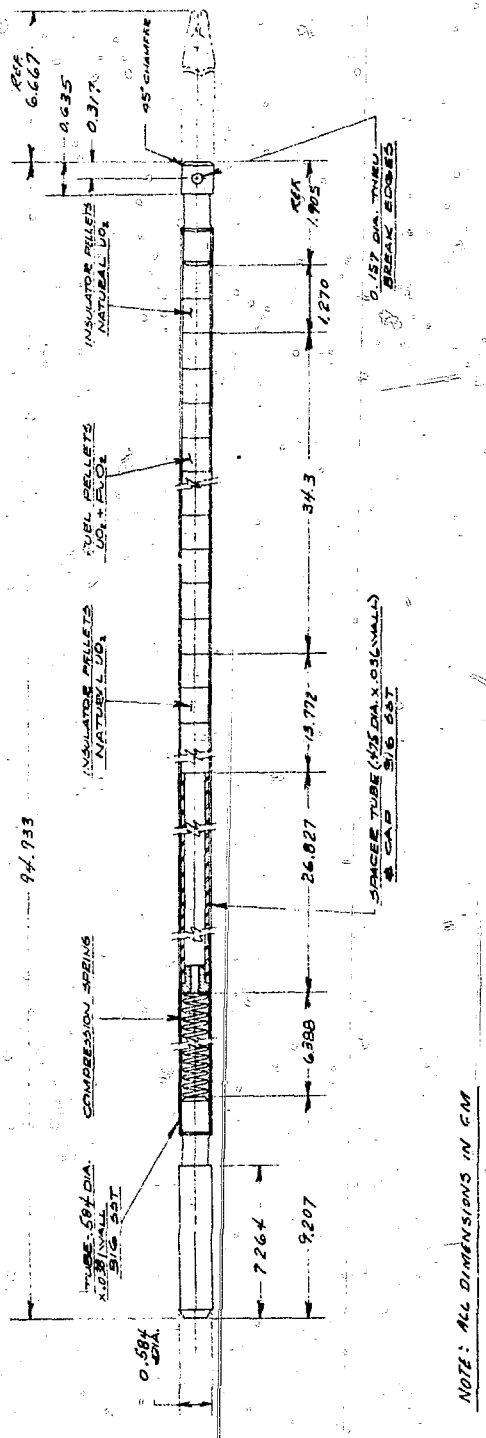

Fig. 4 F-Series Fuel Element, PNL 17A (Modified)

TABLE I F2 Fuel Pin Description

Type	PNL-17A
Pin Number	17A-11
Irradiated	in EBR-II
Irradiated Peak Power	381 w/cm (11.6 kW/ft)
Irradiated Peak Burnup	0.35 a/o
Preirradiation Composition	75% UO_2 - 25% PuO_2
U^{235} Enrichment	80 a/o
Fuel Column Axial Length	34.3 cm. (13.5 in.)
Fuel Microstructural Dimensions (From Sibling Pins at Mid-Axis)	
Central Void Radius	0.66 mm (26 mils)
Columnar Region Radius	2.06 mm (81 mils)
Equiaxed Region Radius	2.21 mm (87 mils)
Unrestructured Region Radius	2.51 mm (99 mils)
Clad Dimensions	
Inner Radius	2.54 mm (100 mils)
Outer Radius	2.92 mm (115 mils)

3.0 POWER GENERATION

The peak linear power rating of the test pin during the F2 test is presented in Fig. 5. Fig. 5 is based upon data from F-series power calibration experiments, and the actual F2 test power generation. Fig. 5 was constructed without considering power generation changes due to changes in fuel geometry after gross axial fuel motion begins at 11 s in the F2 test. Fig. 6 is the relative axial test pin power generation determined by radiochemistry on fuel used in a calibration transient; this figure is normalized, so the relative peak axial power is unity. Relative fuel radial power generation recommended for the F-series is shown in Fig. 7. The radial power profile is based upon radiochemistry performed on concentric cores of a few fuel pellets irradiated in a fueled calibration transient. Cores from the pellets were obtained by an ultrasonic trepanning technique developed by Yaggee[1]. Note that the calibration fuel pellets did not have central voids, but the test fuel pellets had central voids.

The peak linear power rating for the nuclear heated wall was 281 w/cm (8.57 kW/ft) in the nominally flattop power portion of the F2 test transient, as determined by radiochemistry in a calibration transient. Note that this power rating only applies for times before gross axial motion of the test fuel or heated wall. The same axial power shape used for the test fuel is recommended for the heated wall. A ratio of 1.07 was used to describe the ratio of power generation in the outer half of the heated wall compared to the inner half. This ratio was based upon transport calculations performed for the F-series.

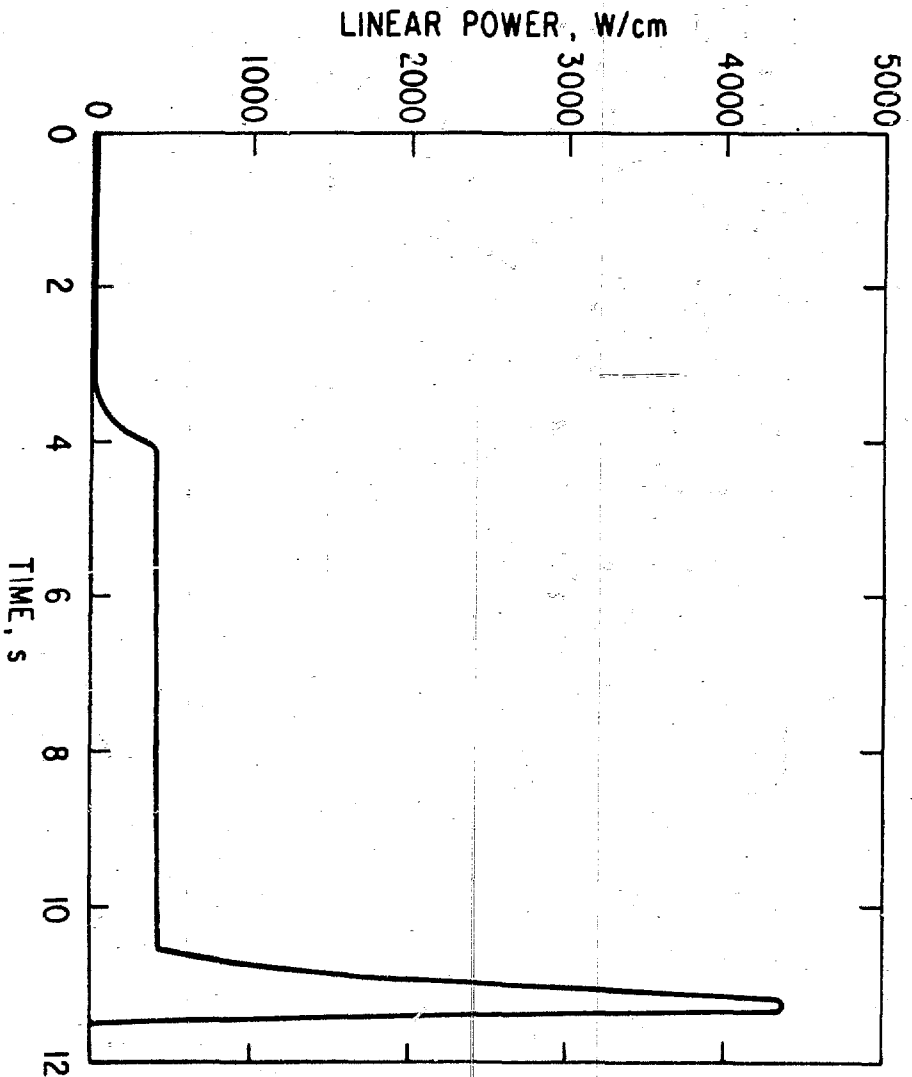

Fig. 5 F2 Test Pin Axial Peak Linear Power Generation

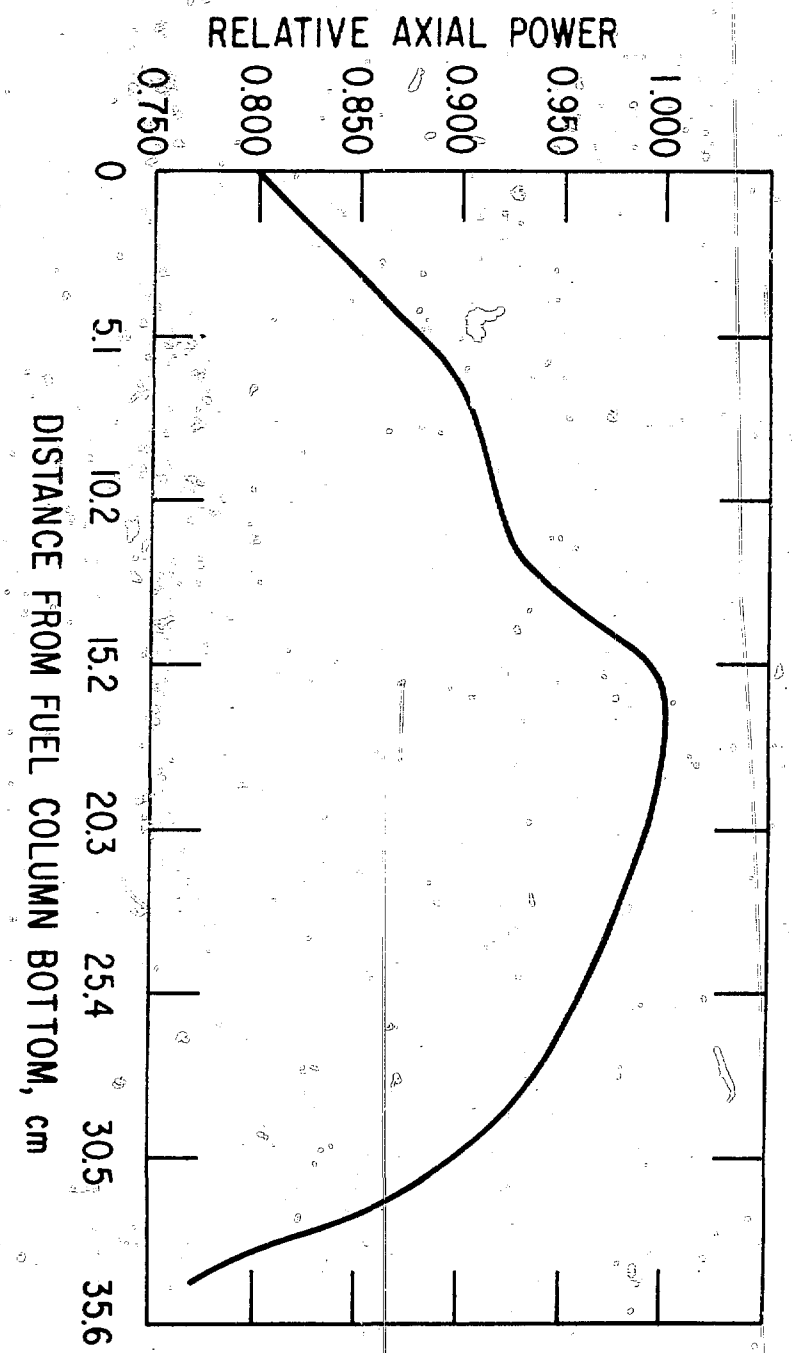

Fig. 6 F-Series Axial Power Distribution from Experiment

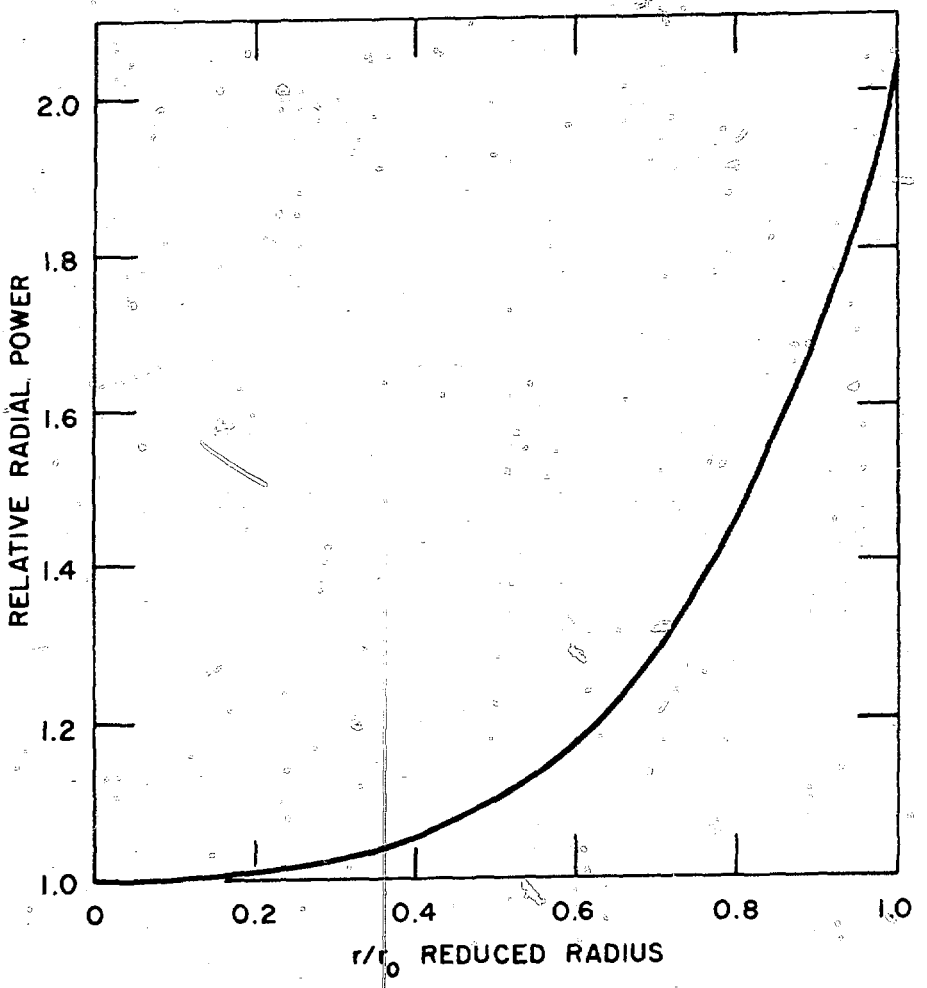

Fig. 7 R-Series Radial Power Profile From Experiment on Unirradiated Power Calibration Fuel
(r_o is outside radius of fuel)

4.0 RESULTS

4.1 Test Capsule Data

Fig. 8 summarizes the test capsule data during and just after the F2 test. Data from the two thermocouples and an idealized TREAT power trace are presented on a common time abcissa in Fig. 8. Appendix A presents plots of raw data that Fig. 8 is based upon. In addition, a plot of the thermocouple and pressure transducer data up to 120 s after test initiation is included in Appendix A.

Both thermocouples burned out during the F2 test. The lower thermocouple located in the tantalum cup below the fuel column burned out at the end of the F2 flattop (~10.5 s). Posttest disassembly of the capsule indicated that molten clad filled the tantalum cup, so contact with molten clad burned out the lower thermocouple. The upper thermocouple burned out while the power was increasing during the power spike. Posttest disassembly of the capsule, the posttest neutron radiograph, and the hodoscope all confirm that the upper thermocouple burned out from contact with molten fuel. Before each thermocouple burned out, their small rises in temperature reflect heatup of the capsule fill gas.

The absolute capsule pressure data shown in Fig.8 is based upon both the absolute capsule pressure before the test, and the change in capsule pressure as sensed by the capsule pressure transducer. The capsule pressure transducer data is not corrected for the negative radiation response of the pressure transducer. This radiation response becomes appreciable after the peak TREAT power. However, the pressure transducer data is judged to be reliable before peak power. This judgement is based upon a radiation response test performed on a similar transducer. A generally smooth rise in capsule pressure over the period of constant TREAT power shown in Fig. 8 reflects a gradual heatup of

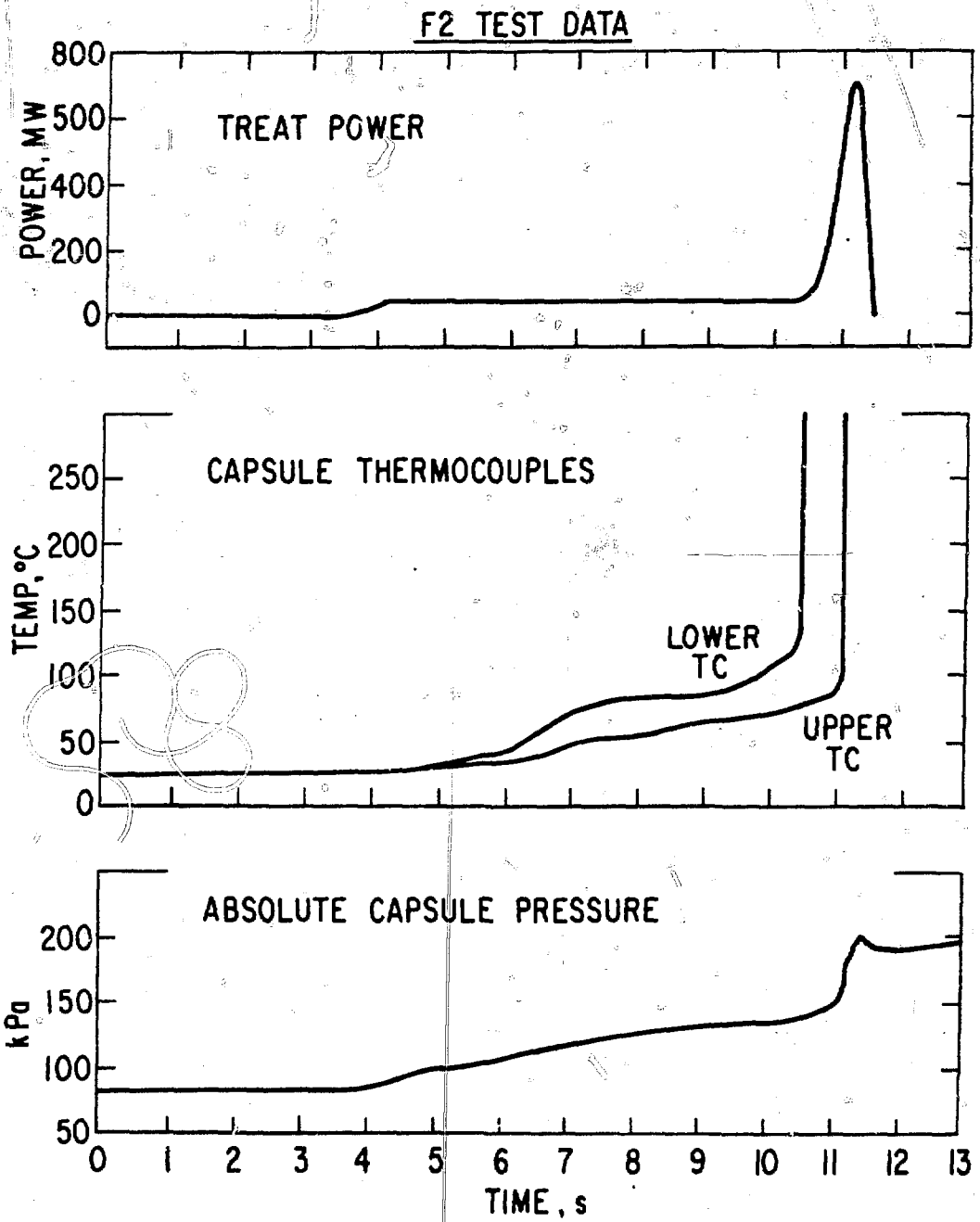

Fig. 8 F2 Test Data

the capsule fill gas. After the power spike begins, the capsule fill gas heated up more rapidly as is shown in Fig. 8.

4.2 Posttest Neutron Radiography and Metallography

The posttest neutron radiograph and two metallographic sections are described in this section. Interpretation of the radiograph is partially dependent upon the incomplete metallographic examination, so the interpretation may be subject to slight changes. The pretest fuel column and the posttest heated-wall axial positions are located on the posttest neutron radiograph (Fig. 9) for reference. A significant feature of Fig. 9 is a 16.5 cm (6.5 in.) long region of molten fuel ejected to a position as high as 19 cm (7.5 in.) above the original fuel column. Most of the ejected fuel is lodged in a 10 cm (4 in.) annular fuel slug located between the insulator pellet region of the fuel pin; and both the tantalum transition piece, and the upper heat sink. Fuel was also driven into two diagonal holes in this region; one in the transition piece, and one in the heat sink. Proceeding downward from the ejected fuel is a 14 cm (5.5 in.) region voided of fuel, a 10 cm (4 in.) region partially voided of fuel, a 8.9 cm (3.5 in.) region of molten fuel extending radially outward to the inside of the heated wall, a 1.3 cm (.5 in.) region partially voided of fuel, and a 1.3 cm (.5 in.) region of partially melted fuel. Test induced changes in the heated wall are evident by its generally deformed shape in the 33 cm (13 in.) long regions either completely voided, partially voided or with molten fuel extending out to the heated wall. Melting of the UO_2 phase in the heated wall, radial deformation of the heated wall out to either the molybdenium reflector or the stainless steel heat sink, and test fuel leakage out of the heated wall were observed in some parts of the previously referred to 33 cm (13 in.) long region. Fig. 9 also shows that the tantalum cup at the bottom is filled with stainless steel clad that drained

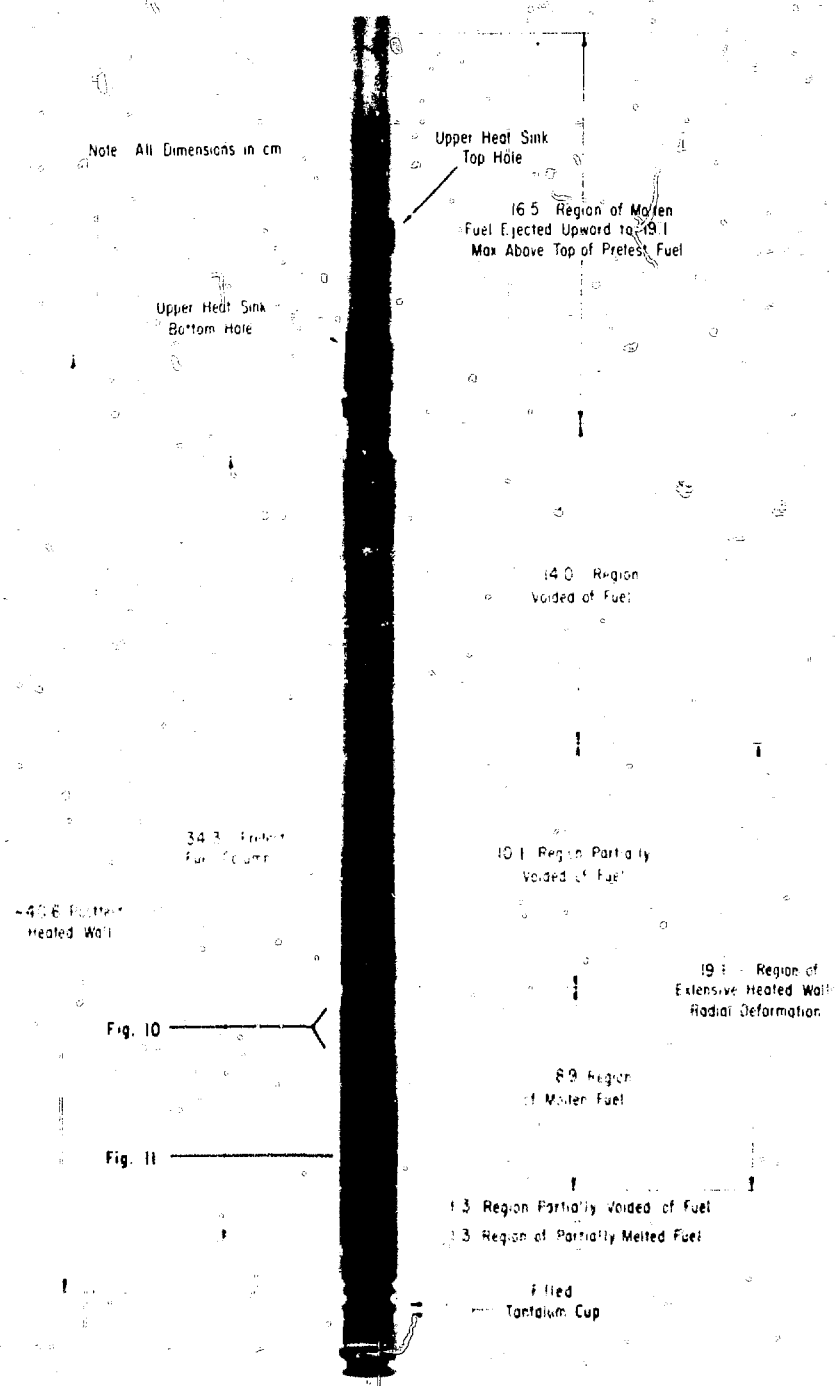

Fig. 9 F2 Posttest Neutron Radiograph

off the fuel column. Figs. 10 and 11 are two metallographic sections taken from the 8.9 in. (3.5 in.) region of molten fuel shown in Fig. 9. The locations of Figs. 10 and 11 are also indicated in Fig. 9. Identification of various test components is made in Figs. 10 and 11. The following observations can be made from the metallographic sections:

- Small metallic particles of varying composition containing Fe-Cr-Ni-W are observed in the fuel.
- A continuous, large central region voided of fuel appears in Fig. 10. No such region appears in Fig. 11, although large voided regions are observed between the fuel and heated wall in Fig. 11.
- The UO_2 phase in the heated wall melted during the test. After the test, some of the molten UO_2 resolidified within the heated wall as large agglomerates. Some of the molten UO_2 may have also migrated out of the heated wall during or just after the test.
- Some radial deformation or erosion of the heated wall is apparent in Fig. 10. Large amounts of test fuel are found outside the heated wall in Fig. 10. This fuel may cause the neutron radiograph interpretation of extensive heated wall radial deformation to be misleading. However, at some axial positions, near the center of the fuel column, the wall did deform out to the reflector.

From the observations made from Figs. 10 and 11, certain comments can now be made relative to the F2 fuel motion behavior. The presence of the Fe-Cr-Ni-W phase in the fuel indicates that there is a potential for fuel dispersal that is driven by clad vapor. However, this clad could have entered the fuel after the first fuel dispersal or even after test scram. The void in Fig. 10 might be interpreted as a vapor pocket in the fuel. Certainly this void is too large to be accounted for entirely by a shrinkage upon solidification.

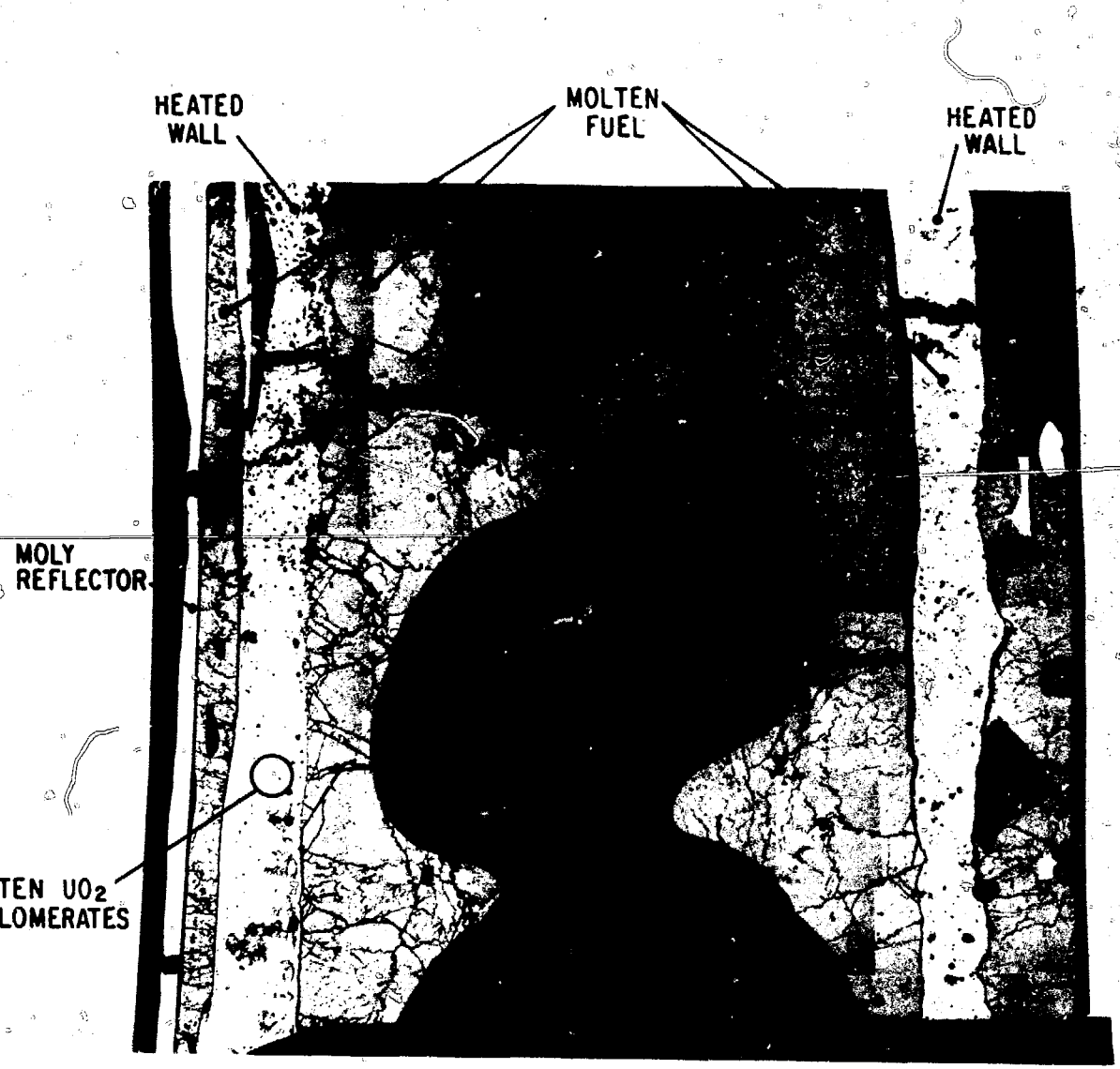

Fig. 10 Logitudinal Section ~9.53 cm (3.75 in.) from Bottom of Fuel Column

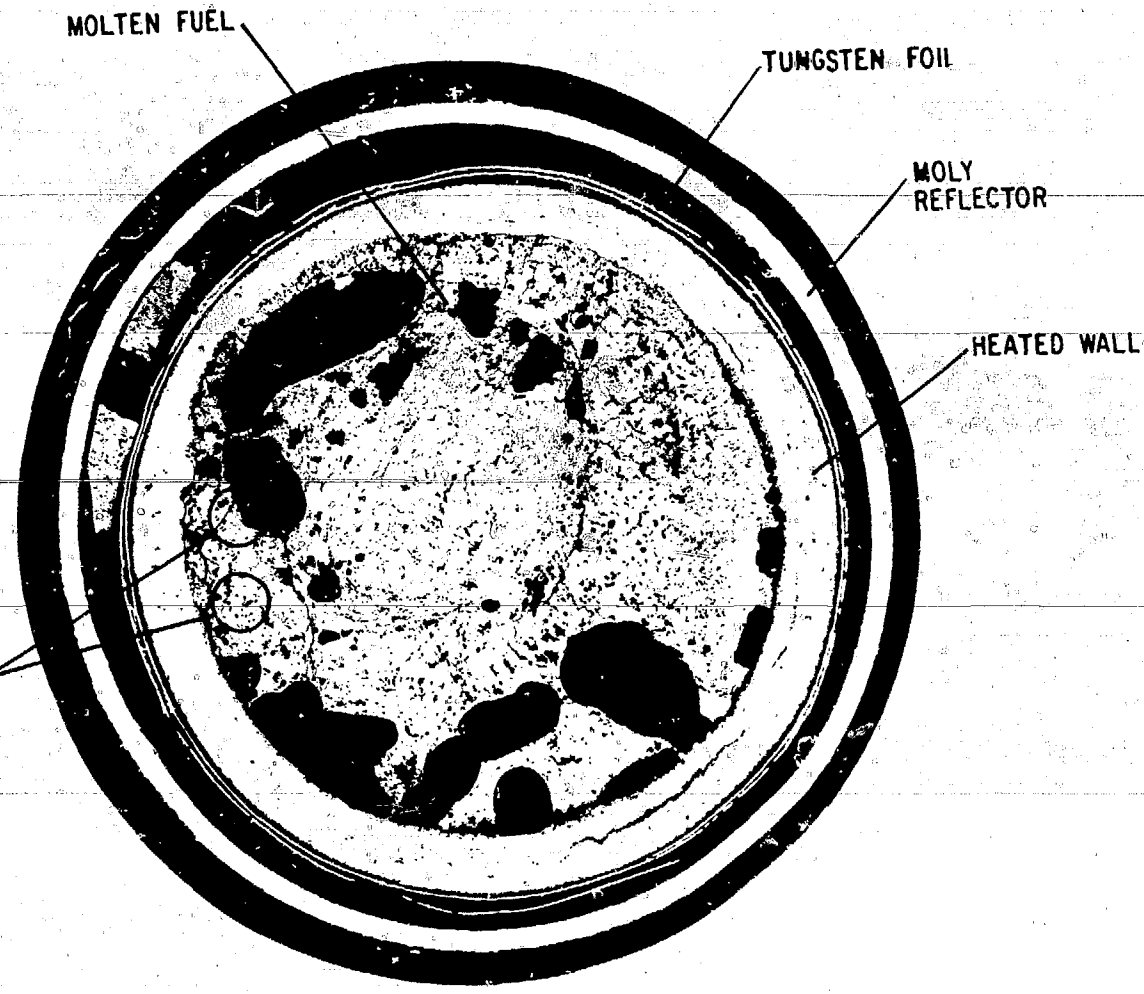

Fig. 11 Transverse Section ~3.81 cm (1.5 in.) from Bottom of Fuel Column

The migration of UO_2 both within and possibly, out of the heated wall after UO_2 melting is quite undesirable. Any future tests using W-UO_2 heated walls should be designed, so the wall does not reach the UO_2 melting point. Radial deformation of the heated wall was probably not too significant an influence on fuel motion. However, leakage of fuel out of the heated wall was significant and might be avoided by wrapping the outside of the heated wall with more layers of W foil. More layers of W foil wrapping might also prevent radial deformation of the wall.

4.3 Hodoscope Results

4.3.1 Summary of Fuel Motion Events

The major fuel motion consisted of an upward dispersal of the top (~10 cm) portion of the fuel pin at 11.04 s. The velocity of the void-fuel interface was approximately 47 cm/sec and the bottom of the ejected fuel reached a height of 19 cm above the center of the fuel pin. At 11.18 s a second event occurred (at approximately the center of the fuel pin) which resulted in an upward movement of an additional 5-8 cm of fuel. Between 11.3 and 12.0 s most of the fuel which had moved upward fell back under the influence of gravity and accumulated in the region around the bottom half of the pin. The final disposition of fuel at 12.4 s is in general agreement with the posttest radiograph. A general summary of the fuel motion as a function of time is shown in Fig. 12. In interpreting this graph it should be noted that the 100% density change indicated in the figure does not consider contributions from the heated wall.

4.3.2 Data Analysis

The hodoscope data has been corrected for the supralinearity of the Hornyak buttons by a computer code SUPRA[2] and for variations in detector efficiencies by the computer code EFFI[3]. Fig. 13 shows a schematic of the

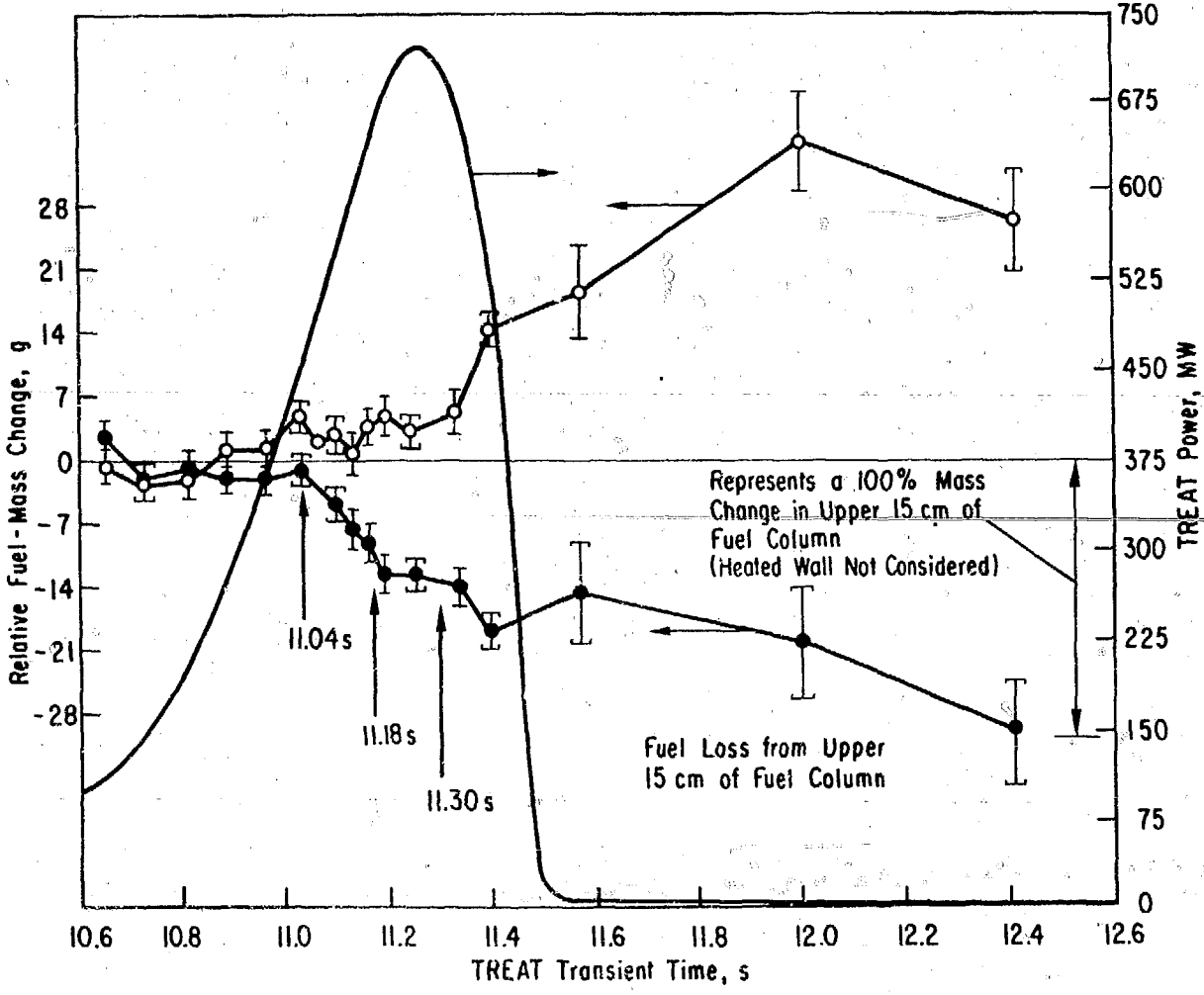

Fig. 12 Fuel Mass Change in Upper and Lower Regions of Initial Fuel Column Relative to Initial Amounts of Fuel Mass in Each Respective Region vs TREAT Transient Time in Test F2, with TREAT Power-burst Profile

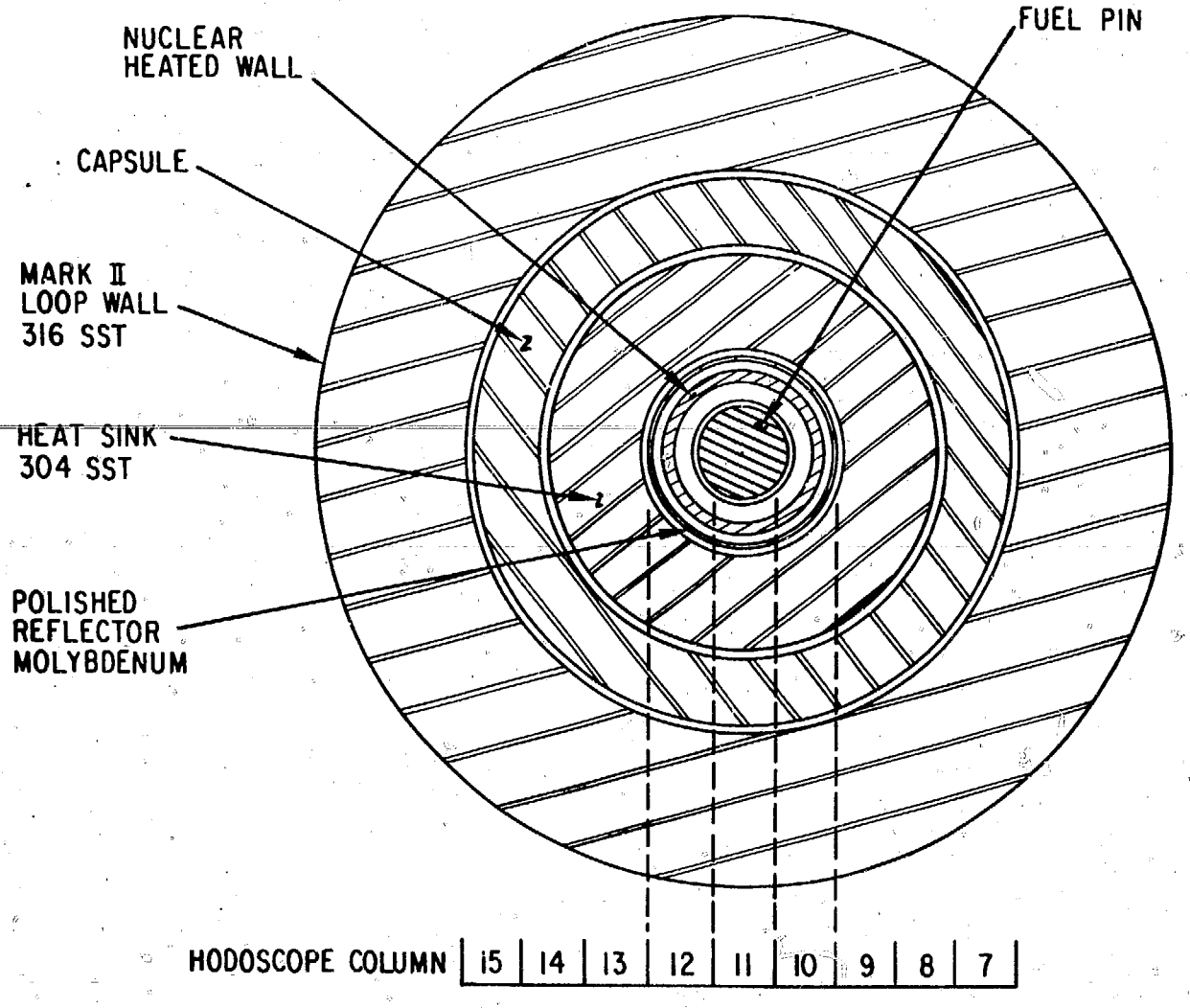

Fig. 13 Schematic of Relationship Between Hodoscope Columns and Test Fuel

relationship between the hodoscope columns and the test fuel. The vertical center of the fuel pin was in row 11.5 and the horizontal center was in column 11.0. The fuel pin extended vertically over 15.3 rows (from row 4.0 to row 19.0) with row 4 corresponding to the top of the pin. In the horizontal direction, the pin extended over three columns (columns 10-12). The orientation of the hodoscope with respect to the reactor is such that the hodoscope is pointed south and column 15 is on the east side of the hodoscope and column 1 is on the west side. The hodoscope view extends approximately 5.3 cm above the top of the fuel pin.

The position of the test pin with respect to the hodoscope field of view had been shifted eastward relative to the nominal pin position. No pretransient scan of the fuel pin (to center the hodoscope) had been made for tests F1 and F2 because of a desire to duplicate the fuel pin position used in F-series power calibration transients. The observed shift indicates that either the test capsule position in the reactor had changed or the hodoscope position indicator had shifted with respect to the earlier tests. This shift resulted in a loss of some information concerning fuel motion in rows 10 and 12 because several scalers were inoperative in the new viewing region. The signal-to-background for F2 was 1.9 which is consistent with F1. The low value of the S/B is probably due to the extra steel in the F-Series test capsule rather than to increased scattering arising from the heated wall.

The main method of measuring fuel motion in this analysis consisted of plotting R/P canges as a function of time. The hodoscope measures the rate, R_F, at which neutrons are emitted from a given mass of fuel. Superimposed on this rate is a background rate of neutrons, R_B, from the reactor and from neutrons scattered by the test capsule. The total rate, R, for a given channel is

$$R = R_F + R_B.$$

Since both the quantities R_p and R_β are porportional to the reactor power, the quantity R/P can be written as

$$\frac{R}{P} = \bar{S} + B \quad ,$$

where $\bar{S}$ is the response from the fuel per unit power and B is the response from reactor background. In general, B is determined by averaging the count rate from a large number of channels which do not view the test fuel. If the assumption is made that the response $\bar{S}$, from a given volume of fuel is proportional to the mass of fuel, M_F, then the previous equation reduces to

$$\frac{R}{P} = KM_F + B.$$

The unknown background can be eliminated by substracting the R/P values at two different times. If t is the time of interest and t_1 is some reference time, then the R/P change between t and t_1 is

$$\Delta(R/P) = \frac{R}{P}(t) + \frac{R}{P}(t_1)$$

$$= KM(t) + B - KM(t_1) - B$$

$$= K\{M(t) - M(t_1)\}.$$

Thus the R/P change between t and t_1 is directly porportional to the fuel motion between t and t_1.

4.3.3 Analysis of Fuel Motion

No fuel motion was observed during the flattop portion of the test transient so the $\frac{R}{P}$ reference value was chosen as the average value of the data between 9.5 and 10.5 s. In order to scope out the general features of the fuel motion, the data for individual scalers were summed. In particular, Figs. 14 and 15 present the $\frac{R}{P}$ change as a function of time for columns 10, 11, and 12 summed over the rows 2-9 and 11-19 respectively. These two figures are useful in showing fuel motion between the upper and lower portion of the

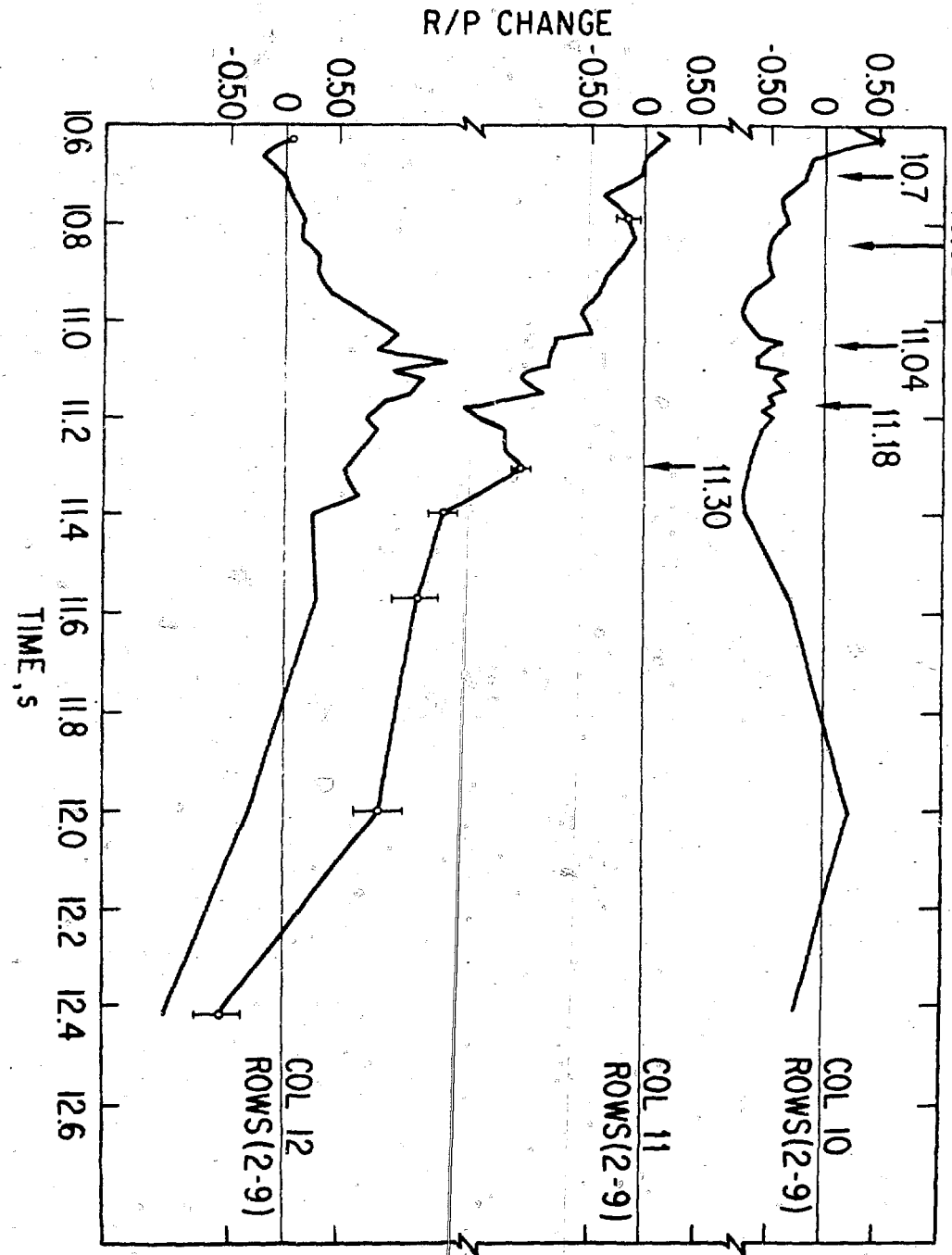

Fig. 14 R/P Changes for the Upper Portion of Columns 10 to 12

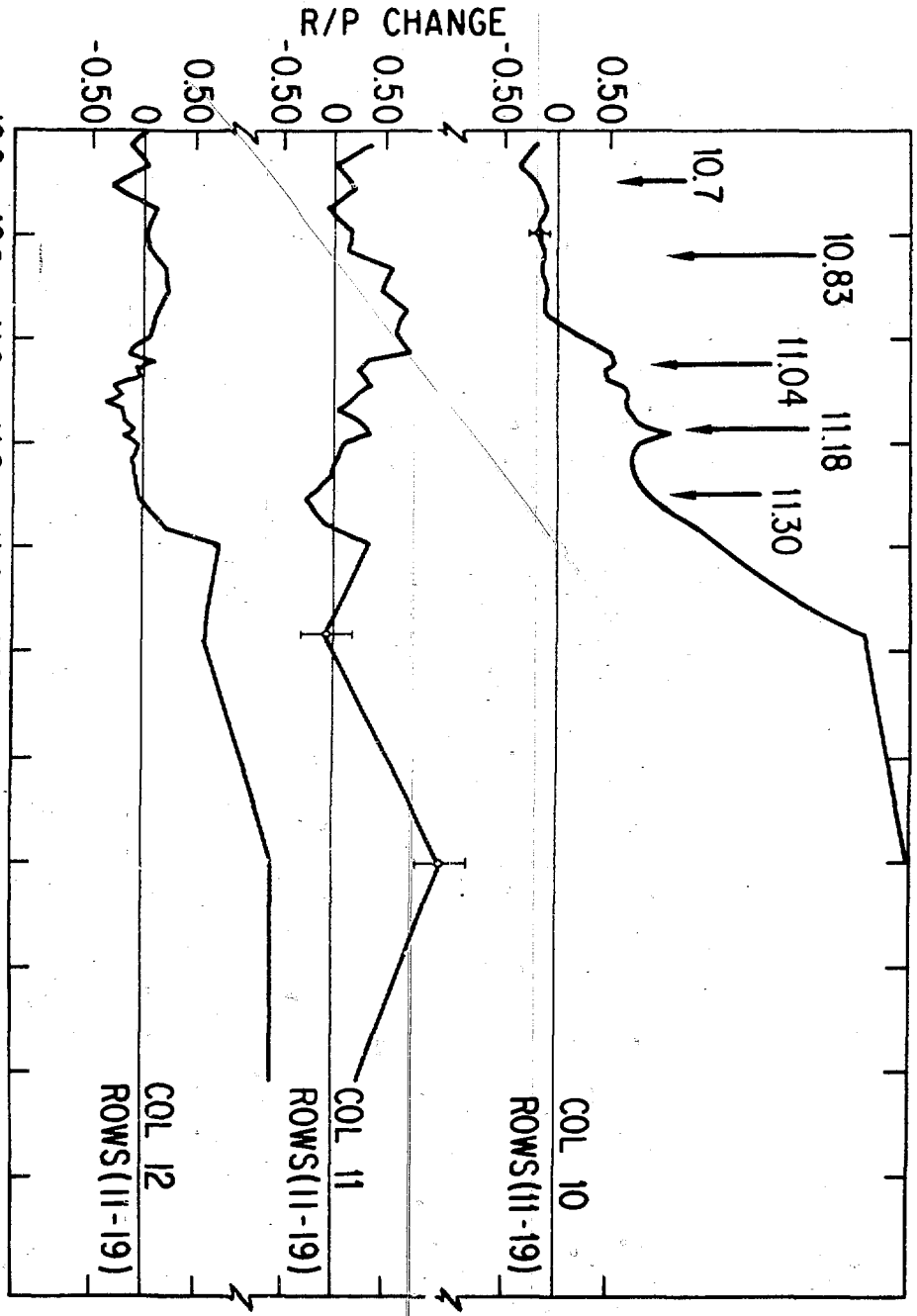

Fig. 15 R/P Changes for the Lower Portion of Columns 10 to 12

hodoscope viewing plane as well as showing fuel motion in a radial direction perpendicular to the hodoscope line of sight. Figures 16 to 19 are R/P change plots of scalers summed over columns 10, 11, and 12. These plots show axial motion of fuel. The error bars in these plots represent statistical errors and do not include systematic errors which may be present. In Figs. 16 to 19, the rows 10 and 12 have been eliminated because of inoperative scalers. An analysis of the data has determined that a R/P change of 1 unit corresponds to a mass of 5±1 gm.

10.7 s. The first indication of fuel motion is indicated in Fig. 14 which shows that at 10.7 s the upper portion of the fuel pin begins to slowly bend toward column 12 (eastward). This shift appears to have reached a maximum value at approximately 11 s.

10.83 s. Fig. 15 shows that an accumulation of fuel begins to occur in the bottom half of column 11 at approximately 10.83 s. The row plots suggest that this accumulation of fuel occurs in rows 11-15 and may represent a filling of the central void since the increase does not occur in columns 10 and 12.

10.98 s. At 10.98 s there appears to be a small event which pushes fuel radially outward from column 11 into columns 12 and 10. This is shown in Fig. 14, in which there is a sudden decrease in column 11 and an increase in the upper portion of columns 10 and 12. At this time there was also an increase observed in rows 4 and 5 of Fig. 16. The top of the fuel pin, as originally positioned, occurred in row 4; thus a slight upward movement of the fuel pin could produce an increase in the count rate for row 4. The increase in row 5 suggests that some fuel may have also been ejected upward at the same time. Analysis of individual scalers suggest that this event was centered in rows 9 and 10 (5.5 to 3.3 cm above the center line of the fuel pin).

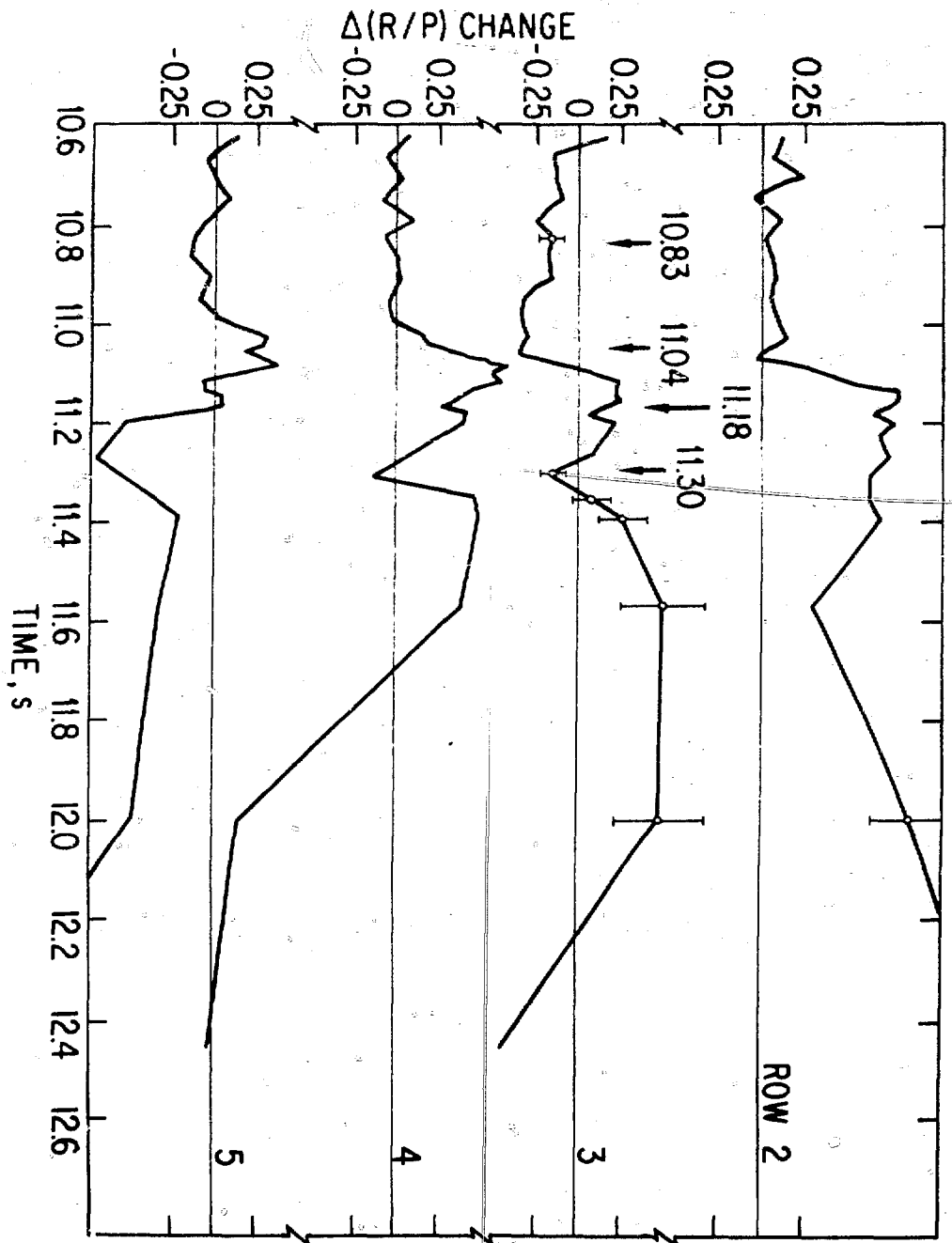

Fig. 16 R/P Changes for Rows 2 to 5 Summed Over Columns 10 to 12

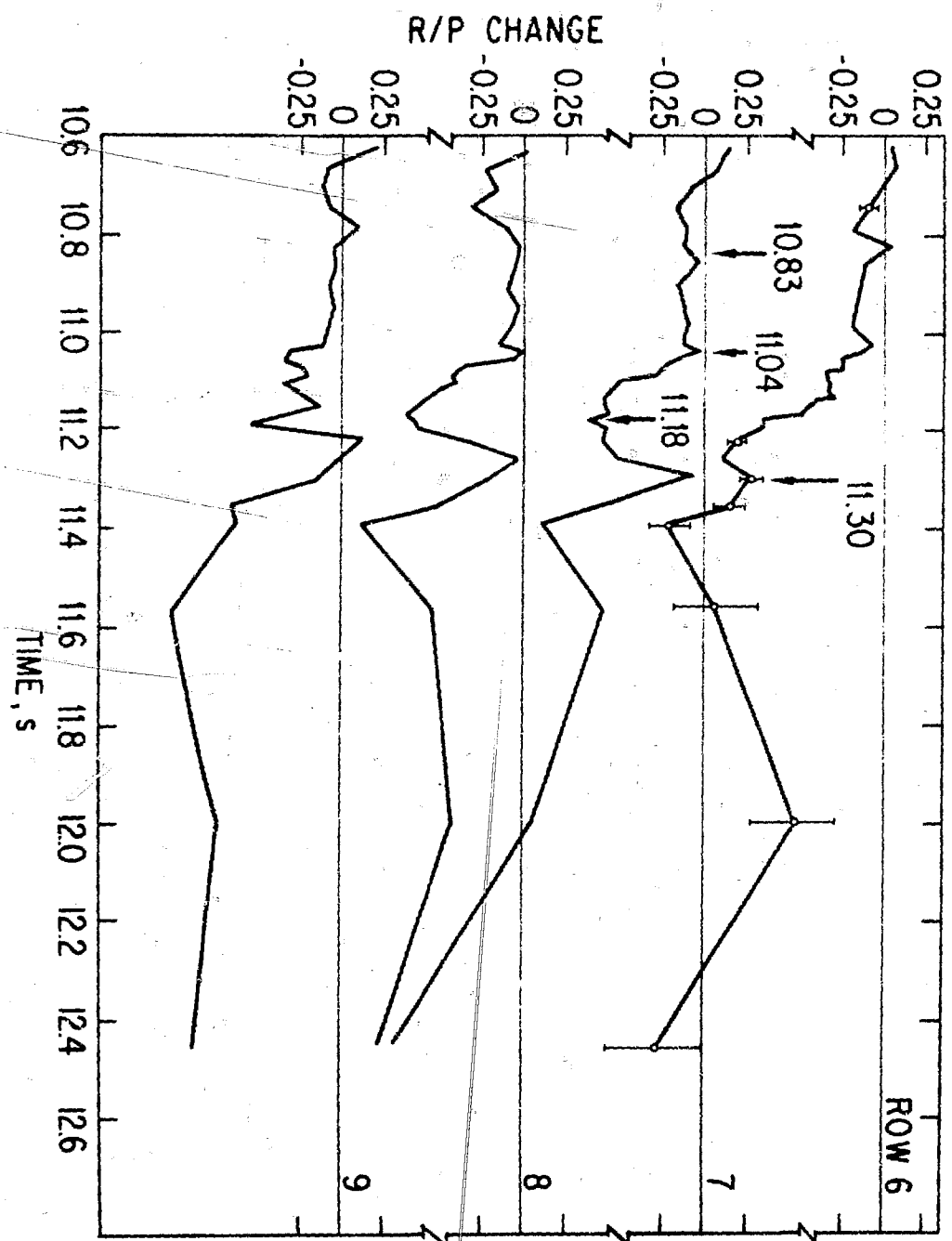

Fig. 17 R/P Changes for Rows 6 to 9
Summed Over Columns 10 to 12

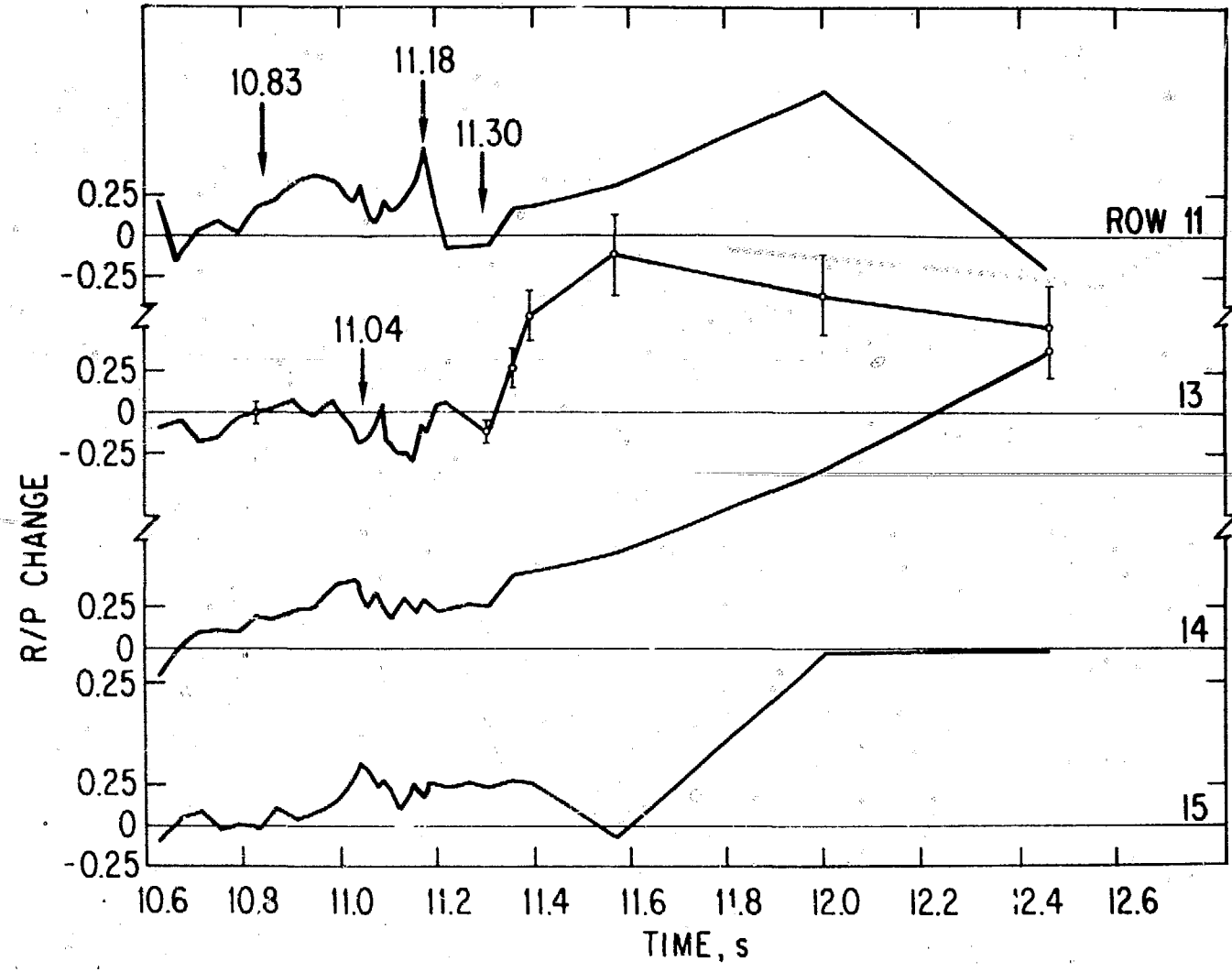

Fig. 18 R/P Changes for Rows 11 to 15
Summed Over Columns 10 to 12

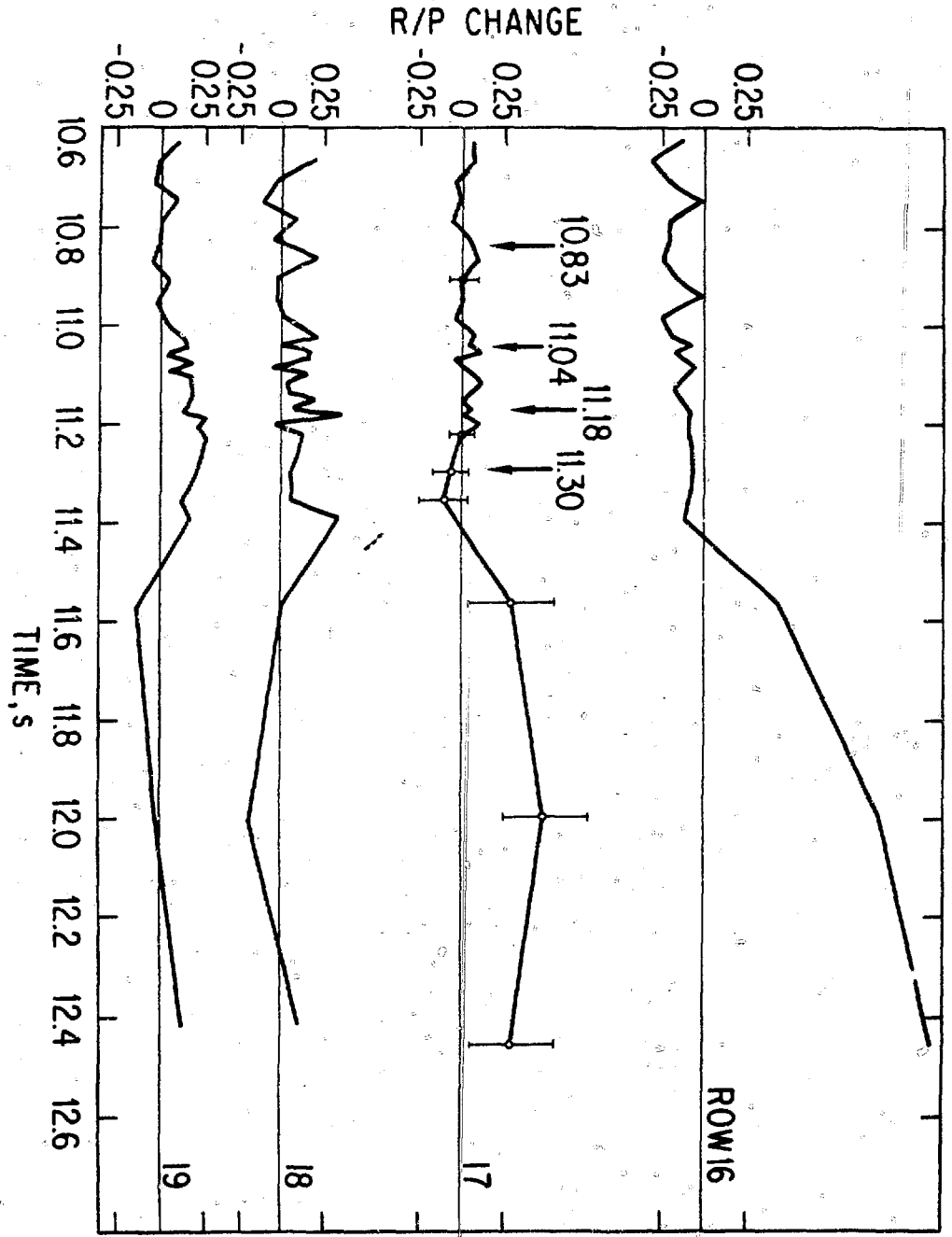

Fig. 19 R/P Changes for Rows 16 to 19
Summed Over Columns 10 to 12

11.04 s. A major event occurred between rows 8 and 9 (6.6 cm above the fuel center line) which resulted in the dispersal of fuel in the top portion of the pin into the upper region of the test capsule. The beginning of this event is indicated in Fig. 17 which shows the voiding of rows 7 and 8 and in Fig. 16 which shows the appearance of fuel in rows 2 and 3. The velocity of the top portion of the void-fuel interface was approximately 47±5 cm/sec. The upper portion of the ejected fuel appears to have moved as a coherent mass. The irregular decrease in the curves for rows 4, 5 and 7 suggest that bottom portion of the void-fuel interface was not well defined or that small amounts of fuel were being lost from the upward moving fuel. Only two-thirds of the original fuel in rows 7 and 8 appears to have participated in the upward movement. Between 11.04 and 11.18 s there is an increase in fuel rows 9-11 which is due to fuel falling or draining of the fuel left in rows 7 and 8. The bottom portion of the upward dispersed fuel reached a maximum height of ∿19 cm (row 3) above the fuel center line at 11.3 s.

11.18 s. A second major event occurred at 11.18 s in the region of the original pin center. Fig. 18 shows that there is a movement of fuel (5-8 cm in length) from row 11 upward into the region vacated by the fuel event of 11.04 s. The fuel involved does not move upward in a very coherent fashion but rather the upward movement of fuel produces a general accumulation in rows 8 and 9 before a major portion of the fuel falls back. Some of the upward moving fuel does reach the bottom of the original blockage in row 3 at 11.3 s before falling back.

11.3 s. At 11.3 s fuel debris begins to accumulate in row 13 (∿3.3 cm below the pin centerline). Fig. 15 indicates that the major portion of fuel increase occurs in column 10 (west side of the pin). The bottom portion of the fuel pin appears to retain its original shape and the fuel which falls from above accumulates between the heated wall and the fuel pin.

11.4 to 12.5 s. After 11.4 s the statistical fluctuations in data became considerably larger and the time averaging of the data had to be greatly increased. The data suggest that after the fuel from the 11.18 s event reached row 3, at approximately 11.3 s, there is a general downward movement of fuel under the influence of gravity. Some of the fuel corresponds to that ejected upward at 11.18 s, but there is also some additional fuel from the original blockage. At 12.4 s the data is qualitatively similar to the post-test neutron radiograph.

4.3.4 Discussion

In test F2, the ratio of the number of neutrons produced in the heated wall to that in the fuel pin was ~0.65. Calculations involving the hodoscope response show that the heated wall had only a 20% effect on the S/B ratio for the hodoscope column 11 which was centered on the fuel pin, and approximately a 100% effect on columns 10 and 12 which were positioned on either side of the fuel pin. These variations in the S/B appear to have had little effect on the qualitative measurements and interpretation of the fuel motion. The actual quantitative information on the total quantity of fuel which was involved in the fuel motion is more complex, however, because of melting of a portion of the heated wall.

5.0 THERMAL AND FUEL EJECTION ANALYSIS

5.1 Radial Temperature Profiles

Fig. 20 presents calculated radial fuel temperature profiles for the peak power (mid-axis) segment of the F2 fuel column. Calculations were performed using a version of the THTB general purpose heat transfer code maintained at ANL. Important features of the THTB model include heat transfer by radiation between the fuel, and heated wall; the heated wall, and heat shield; and the heat shield, and the heat sink. Table II keys the test times for each profile with comments on the selected times. Because the large radial flux depression causes more power to be generated near the pellet edge than near the center (see Fig. 7), the F2 fuel thermal gradients are quite low. The highest thermal gradient was calculated at 7.90 s just after the clad was calculated to melt. Passage of the clad through its heat of fusion causes a pause in the temperature rise near the pellet edge compared to the pellet center. Therefore, clad melting establishes the maximum temperature gradient in the F2 test. By 9.23 s the clad has been assumed to disappear, and the temperature gradients at the pellet edge have diminished. At 10.53 s, the constant power portion of the F2 test transient has just ended. By 10.73 s, fuel had just started to melt at mid-radius. At 11.05 s, (the fuel ejection time), all the fuel was calculated to be at or above the solidus temperature. Peak temperature at 11.05 s was ~5000°C. It must be stressed that the temperature profiles after the fuel melting has begun are calculated for the pre-melted fuel geometry, and therefore do not reflect possible changes in the energy deposition due to molten fuel rearrangement.

5.2 Initial Fuel Ejection Event Analysis

The hodoscope and the heat transfer calculations indicate the fuel column was erect and not yet molten at the beginning of the power spike (~10.5 s).

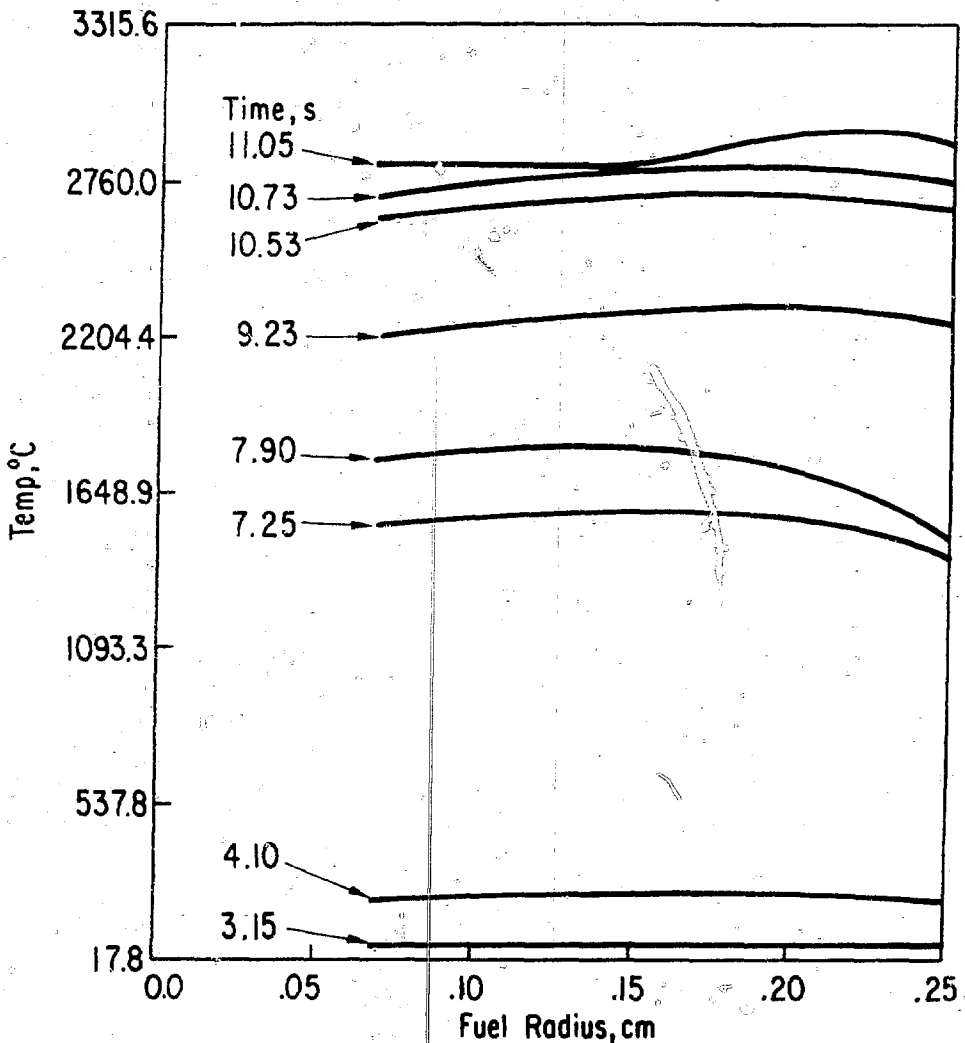

Fig. 20 F2 Fuel Radial Temperature Profiles

TABLE II Key to F2 Radial Temperature Profiles

Test Time, s	Comment
3.15	Begin approach to power flattop from cold capsule conditions.
4.10	Begin constant power.
7.25	Begin clad melting.
7.90	End clad melting.
9.23	
10.53	Start F2 power spike.
10.73	F2 fuel starts to melt.
11.05	Temperature profile at time of the pressure event that ejected fuel upward.

In addition, burnout of the lower thermocouple at this time indicates that most of the clad had drained off the fuel column. Between the power spike initiation time, and the peak TREAT power at 11.234 s, molten fuel was ejected at 11.04 s above the top of the original fuel column. Timing of the initial ejection was verified by burnout of the upper thermocouple and hodoscope observations. The purpose of this analysis is to estimate what absolute pressure existed in the test fuel at the time of the initial fuel ejection. From the pressure estimate, and the heat transfer calculation (Section 5.1), an attempt is made to identify what vapor species drove the initial ejection.

Fig. 21 is a schematic of the relevant test components that were involved in the initial fuel ejection. This figure shows the region around the ∿10 cm long annular slug of ejected fuel that froze in the cool upper structure just after the first ejection event. This ejected slug is also visible in the posttest neutron radiograph (Fig. 9).

The absolute pressure in the ejected fuel was determined in the following manner. This absolute pressure was estimated from the sum of the three pressures listed below:

1. The absolute pressure of the helium capsule fill gas at the beginning of the test.
2. The change in capsule pressure, as determined by the pressure transducer mounted at the top of the capsule, prior to the ejection event. This pressure change is mainly due to thermal expansion of the capsule fill gas.
3. The pressure difference ($P_L - P_U$) necessary to drive the ejected molten slug upward just before fuel freezing prevented further upward motion. P_L and P_U are the pressures below and above the ejected slug as indicated in Figure 21.

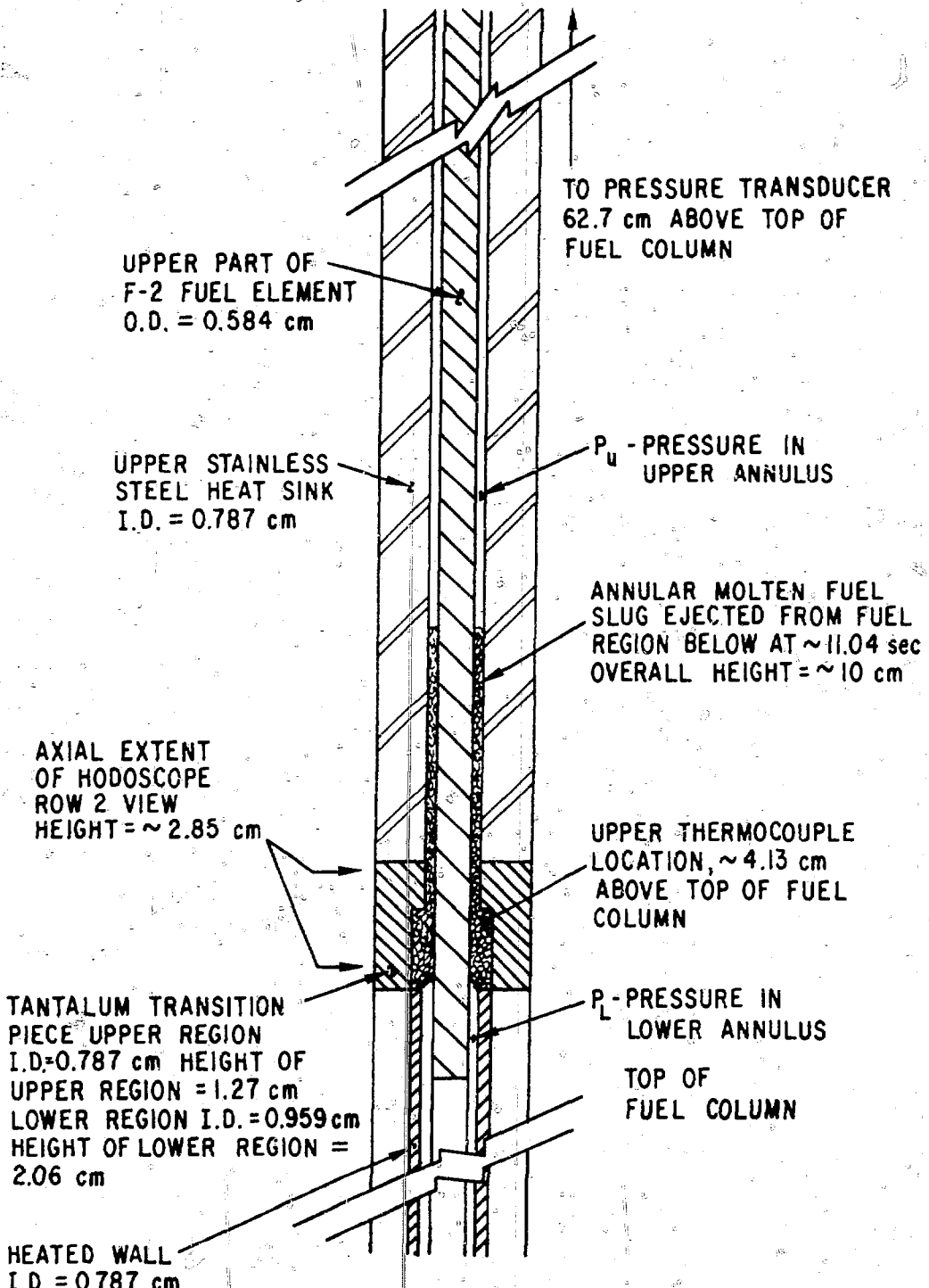

Fig. 21 Schematic of F2 Ejected Fuel Slug

The sum of the first two pressures above is P_U. P_L is the pressure that is of most interest, since it is the absolute pressure below the ejecting fuel slug. P_U is a measured quantity and is known to a good degree of confidence. (P_L - P_U) can be crudely estimated from indirect considerations. Fortunately, (P_L - P_U) is small compared to P_U so P_L is also known to a good degree of confidence. An estimate of (P_L - P_U) can be made in the following manner. This pressure drop is the sum of the static pressure head needed to eject a slug 10 cm high and a frictional pressure loss associated with the fuel motion. Calculation of the static pressure head is straight forward and is 7.8 kPa. In order to estimate frictional pressure loss, some knowledge of the fuel slug velocity is necessary. During the ejection event, the upper surface of the slug passed through row 2 of the hodoscope resulting in a large increase to the hodoscope signal in a short period of time ($\Delta\tau$). From a knowledge of the axial distance or height (h) over which the hodoscope row is sensitive to fuel motion, the velocity (v) of the advancing slug may be estimated from the following:

$$v = h/\Delta\tau = 47 \pm 5 \text{ cm/sec}$$

Unfortunately, as seen from Fig. 21, this velocity is averaged over two flow areas. However, row 2 is situated so that its axial response should be more sensitive to motion in the larger flow area. Therefore this velocity will be assumed to be representative of the velocity in the larger flow area. Assuming a constant mass flow rate for the fuel slug until freezing occurred, the time that the fuel slug took to freeze may be estimated from the hodoscope measured velocity, continuity, and the fuel slug height measured from the neutron radiograph. Using dimensions from Fig. 21:

$$\tau_f = \frac{2.06 \text{ cm}}{47 \text{ cm/sec}} + \frac{10 \text{ cm} - 2.06 \text{ cm}}{47 \text{ cm/sec} \times \left[(.940 \text{ cm})^2 - (.584 \text{ cm})^2\right]} \Big/ \left[(.787 \text{ cm})^2 - (.584 \text{ cm})^2\right]$$

$$\tau_f = 0.04 \text{ s} + 0.08 \text{ s} = 0.12 \text{ s}.$$

As a partial check upon the assumptions used to calculate τ_f, a heat transfer calculation of the time necessary to clog the molten fuel flow due to freezing was made. Clogging probably first occurred in the narrow part of the annulus at the bottom of the stainless steel heat sink. Because the initial temperature of the heat sink was cold (~150°C) compared to the molten fuel, ablation[5] of the steel need not be considered. A simple THTB model consisting of the upper part of the fuel element, a static 10 node molten fuel slug, and the stainless steel heat sink was used to calculate the freezing times for various initial fuel temperatures. Results of the heat transfer calculations are presented below:

Time to Clog Fuel Flow Due to Fuel Freezing	Initial Fuel Temperature
Sec.	°C
0.190	3300
0.140	3000
0.100	2770*

The times listed above are the times that the last fuel node fell below the liquidus temperature. Note that the freezing times are not sensitive to initial fuel temperature since most of the heat transferred to the heat sink is contained in the heat of fusion. The time necessary to clog the fuel annulus τ_f calculated previously and the times for fuel freezing based upon the heat transfer calculation are both about 100 msec. This agreement enables us to use the hodoscope measured velocities and the final slug height to calculate with some degree of confidence the frictional pressure loss from Darcy's law just prior to freezing. The frictional pressure loss in 2.2 kPa. Therefore the total pressure drop ($P_L - P_L$) due to both the static pressure

*Slightly above fuel liquidus.

head plus frictional losses is 10 kPa. P_U at the time of fuel ejection was 142 kPa. As mentioned previously, $(P_L - P_U)$ is small compared to P_a, so the crude estimate of $(P_L - P_U)$ suffices to estimate P_L. P_L at the time of the ejection then is 152 kPa (22 psi).

Heat transfer calculations of the peak power axial segment in the F2 fuel at various times during the test have been reported in Section 5.1. At the time of the initial fuel ejection, the peak temperature was calculated to be ~3000°C. Less confidence is placed in the heat transfer calculation compared to the absolute pressure calculations because as previously mentioned the heat transfer calculation is likely to be more sensitive to changes in fuel geometry after fuel melting begins.

At this point in the analysis, both an absolute pressure of 152 kPa (22 psi) and a maximum fuel temperature of 3000°C in the ejected fuel have been calculated. One question that naturally arises is whether the pressure and temperature are consistent with the saturation pressure or vapor pressures of candidate species that could be responsible for the F2 fuel dispersal. Table III shows that all the candidate species for the F2 ejection cannot be rejected from thermodynamic considerations. However, fuel vapor may have caused the fuel ejection because fission products and stainless steel might not have been intimately mixed in the fuel at ejection time. High temperatures could have released most of the fission products before the ejection, and there is evidence that most of the stainless steel had drained off the fuel column prior to the power burst. Some clad material was found in the fuel in the posttest examination. However, there is no way of knowing when this clad entered the test fuel.

TABLE III Properties of Candidate F2 Dispersal Species at 152 kPa (22 psi) or 3000°C

Candidate Species	Saturation Temperature at 152 kPa	Vapor or Gas Pressure at 3000°C	Comment
	°C	kPa	
Mixed Oxide	3300[6]		Heat transfer calculation of 3000°C is low compared to saturation temperature of 3300°C. However, the 300°C discrepancy is within the range of uncertainty of the heat transfer calculation.
Cesium		540	This value is from Gabelnick and Chasanov[7] and is interpolated for both burnup and temperature. 100% retention of the fission products at the time of fuel ejection is also assumed in Gabelnick and Chasanov's analysis; this is likely to grossly overestimate the fission product pressures at 3000°C.
Xenon		840	Same comment as for cesium applies.
Stainless Steel (Cladding)	2903[6]		This saturation temperature comes closest to agreement with the heat transfer calculation. However, most of the cladding had drained off the fuel column before the fuel ejection event.

6.0 PRELIMINARY CONCLUSIONS

The following conclusions can be made based upon the posttest neutron radiograph, preliminary hodoscope data analysis, preliminary thermal analysis, and an incomplete posttest examination:

- Some fuel dispersal to regions above the original fuel column position occurred in Test F2.
- The vapor species that drove the initial fuel dispersal cannot be unambiguously identified as yet. However, fuel vapor is a strong candidate for the dispersal species.
- The heated wall did not contain the test fuel in an optimum manner by the time of test power scram. However, it is possible that the heated wall test fuel containment was adequate at the time of the initial test fuel dispersal.

REFERENCES

1. F. L. Yaggee and G. Dragel, "An Ultrasonic Trepanning Technique for Radial Sampling of Ceramic Fuel Pellets for Fission Analysis," Trans. Am. Nucl. Soc., 19, 263 (1974).

2. C. L. Fink, ANL, private communication.

3. E. A. Rhodes, ANL, private communication.

4. J. J. Kaganove, ANL, private communication.

5. M. Epstein, "Heat Conduction in the UO_2 Cladding Composite Body with Simultaneous Solidification and Melting," Nuclear Science and Engineering, 51, 84-87 (1973).

6. ANL-CEN-RSD-76-1, Properties for LMFBR Safety Analysis, April 1976.

7. S. D. Gabelnick and M. G. Chasanov, "A Calculational Approach to the Estimation of Fuel and Fission-Product Vapor Pressures and Oxidation States to 6000°K," ANL-7867, October 1972.

APPENDIX A

Test Instrumentation Raw Data

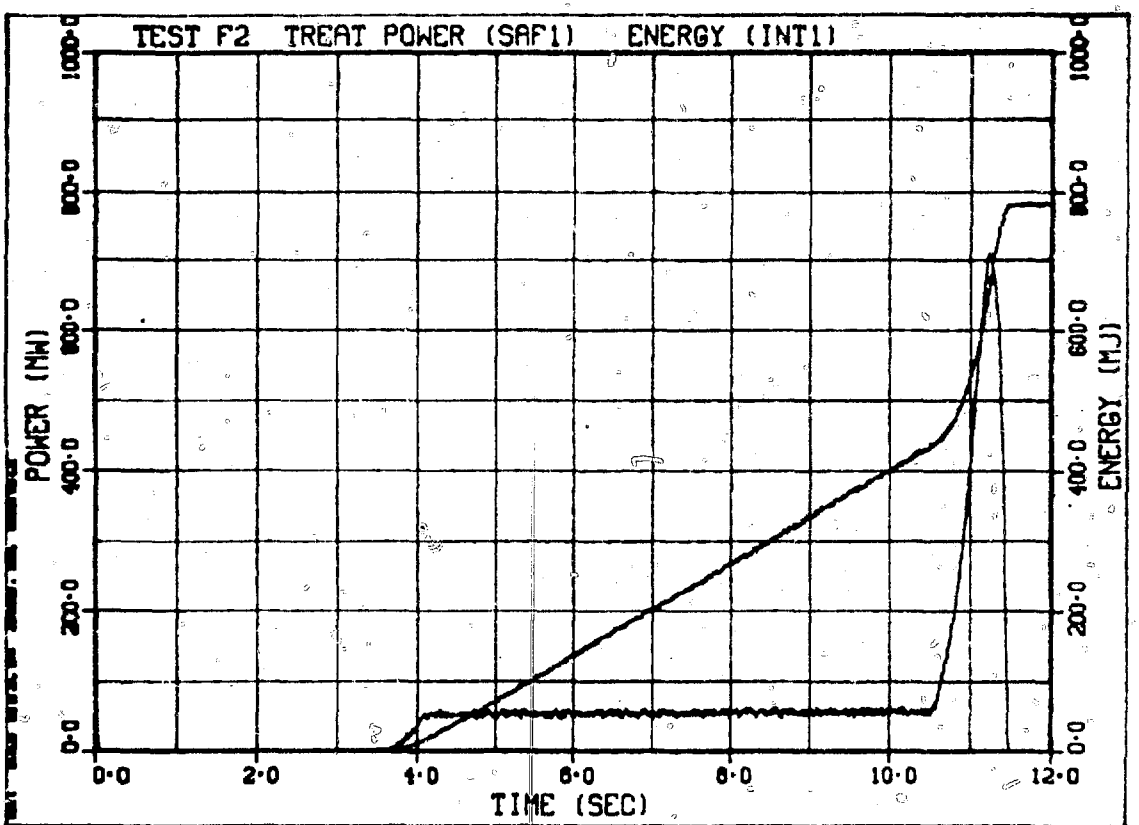
TEST F2 TREAT POWER (SAF1) ENERGY (INT1)
POWER (MW)
ENERGY (MJ)
TIME (SEC)
0·0
200·0
400·0
600·0
800·0
1000·0
2·0
4·0
6·0
8·0
10·0
12·0

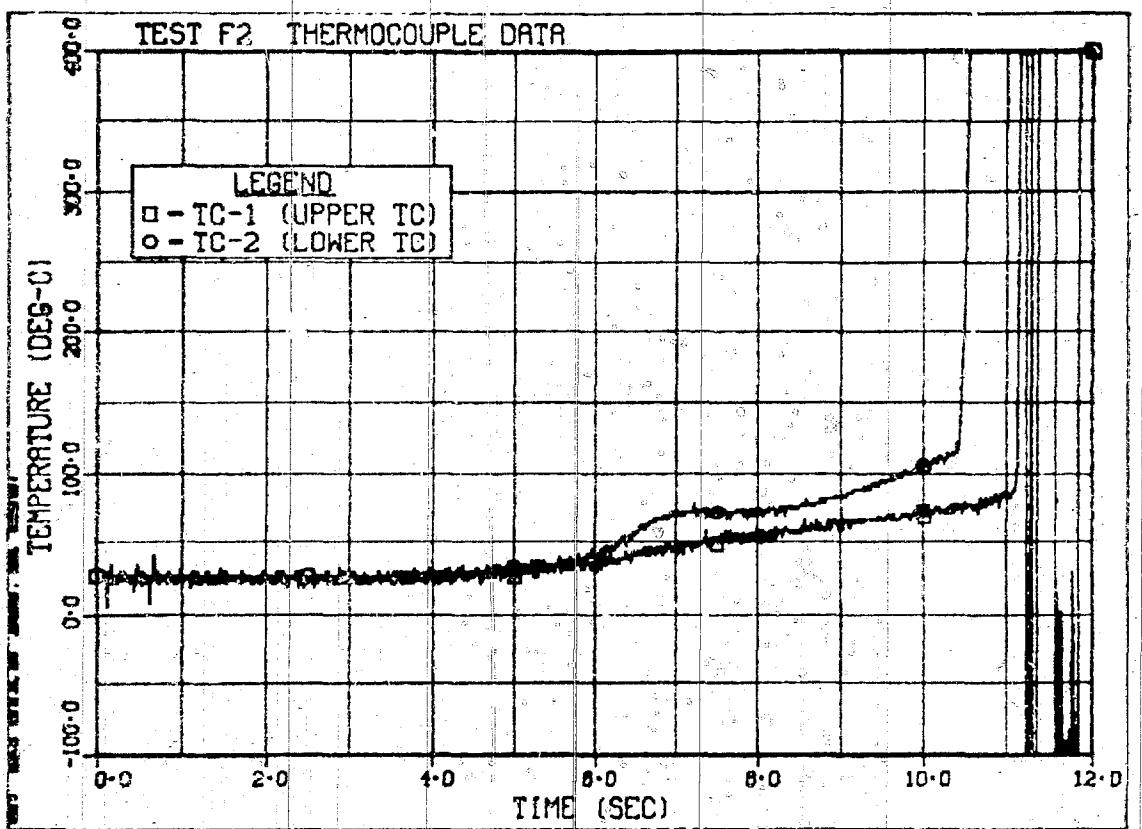
TEST F2 THERMOCOUPLE DATA
LEGEND
□ - TC-1 (UPPER TC)
○ - TC-2 (LOWER TC)
TEMPERATURE (DEG-C)
400·0
300·0
200·0
100·0
0·0
-100·0
0·0
2·0
4·0
6·0
8·0
10·0
12·0
TIME (SEC)

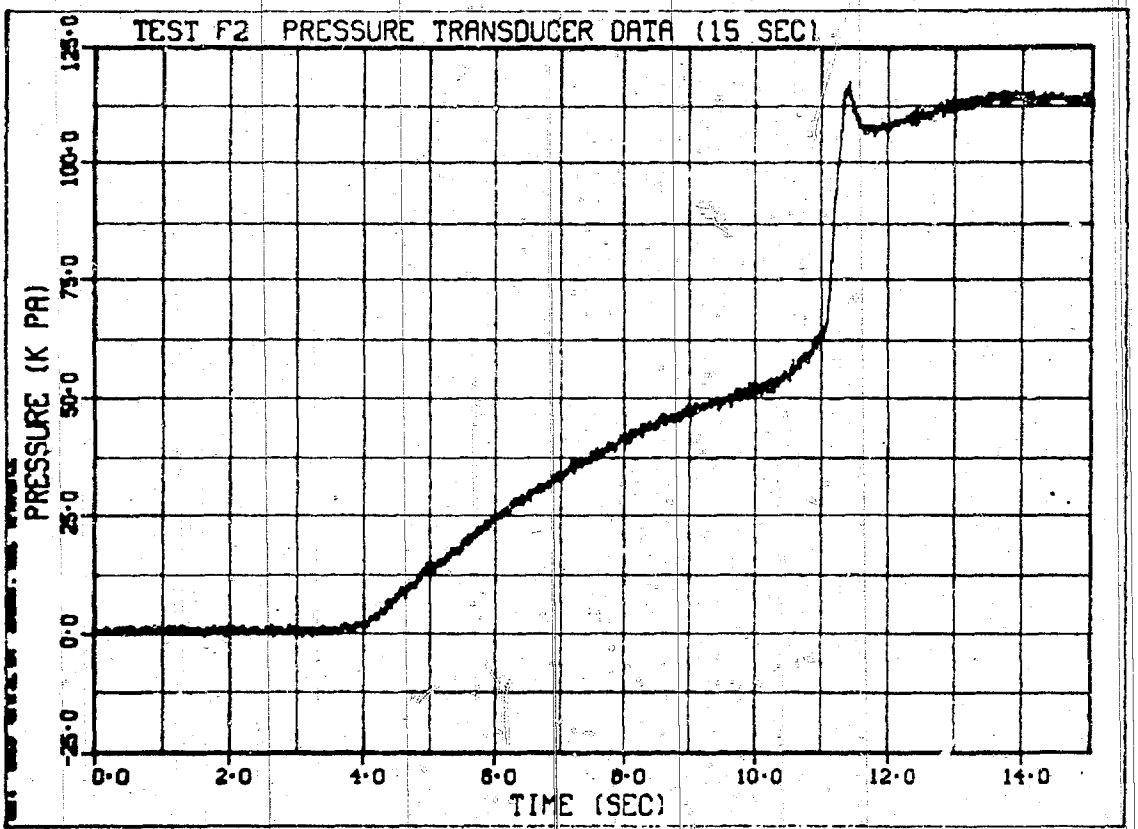
TEST F2 PRESSURE TRANSDUCER DATA (15 SEC)
PRESSURE (K PA)
125·0
100·0
75·0
50·0
25·0
0·0
-25·0
0·0
2·0
4·0
6·0
8·0
10·0
12·0
14·0
TIME (SEC)

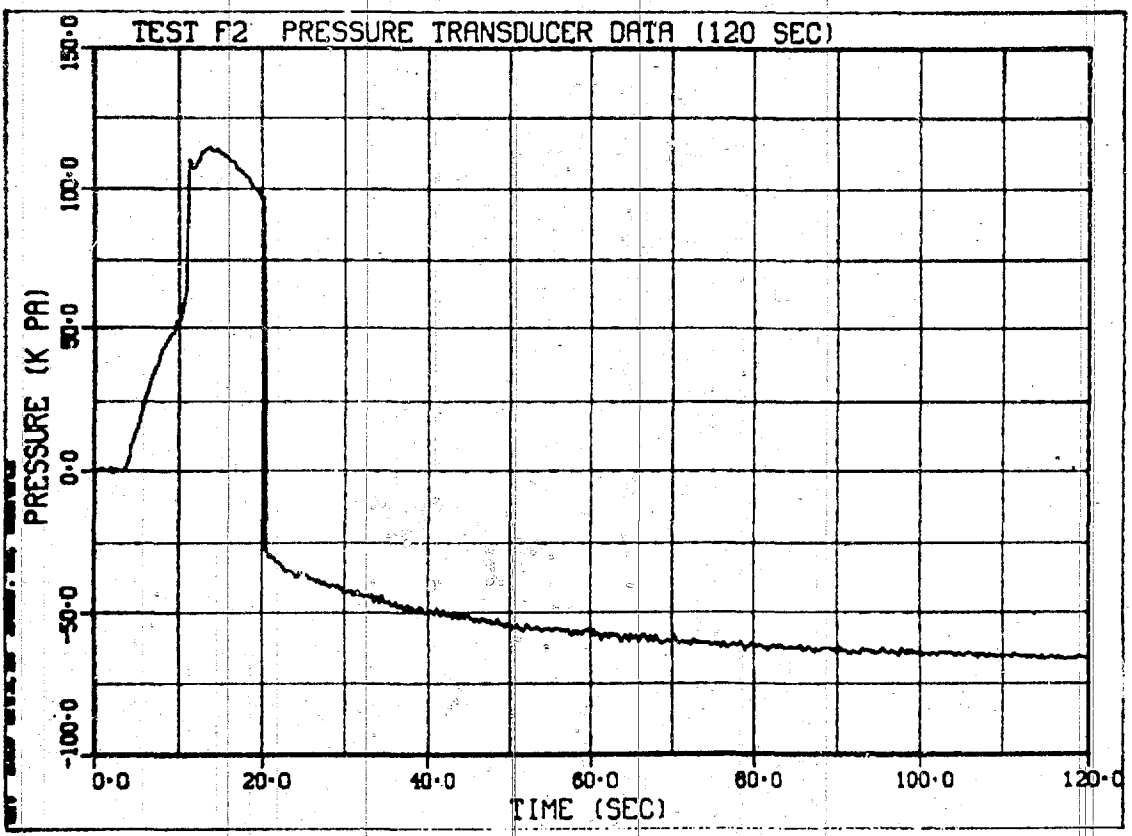
TEST F2 PRESSURE TRANSDUCER DATA (120 SEC)
PRESSURE (K PA)
150·0
100·0
50·0
0·0
-50·0
-100·0
0·0
20·0
40·0
60·0
80·0
100·0
120·0
TIME (SEC)

ACKNOWLEDGEMENTS

The execution of the F2 test and the F-series power calibration tests depended on contributions from many persons at Argonne. The overall direction of the program was the responsibility of Charles Dickerman. Bob Noland was responsible for test hardware and experiment operations. Larry Harrison, at TREAT, provided the facility management for running the test.

Special mention must be given to Chuck McPheeters and Verne Kolba, who served as lead experimenter and test designer respectively, during the conceptual and power calibration stages of the F-series.

Paul Basnar assisted in design of the F-series and also created the engineering drawings. Operations Group Leader, Neill Carson, and Test Engineer, Dick Purviance, supervised the assembly of the F-series hardware. Jim Emerson assembled the F-series test trains. Special mention to Paul Basnar, Neill Carson, Dick Purviance, and Jim Emerson is in order for making last minute changes in the test design and still meeting the schedule. Gene Maslowicz and Joe Burghardt outfitted the F-series Mark II-A loops. Ken Schmidt, Jerry Dewey, Charley August, and Bob Mailhoit also assisted with the F-series hardware. Lindy Willis handled the shipping of the test hardware between Illinois and Idaho. Fuel and HFEF coordination was handled by Howard Rhude. George Trahey and Lew Garrison were the Q/A representatives. Typing of this report was by Rosie Tooley. Pam Parks, Liz Rooney, Barbarba Cobb, and Kathy Rank typed the volumes of information needed to execute the F-series tests.

Mark Stephenson performed many heat transfer and reactor kinetics calculations for the F-series. Mark also wrote the F-series safety report. Gerry Klotzkin and Jack Ulrich performed Monte-Carlo and transport neutronic calculations for the F-series. Frank Yaggee, Gabe Dragel, and Roland Armani

devised and executed an experimental method of obtaining the radial power profile used for the F-series. Extensive radiochemical work for the calibration tests was performed by Earl Ebersole and Bob Villareal. Earl Ebersole was also quite helpful in explaining the precision and accuracy that could be expected from the radiochemical determinations. Paul Froehle digitized the F-series data after the F1 and F2 tests and prepared the graphs of the raw test data.

At HFEF; Jay Cook, Ken Teraguchi, and Jim Kerr worked on the hot cell operations needed to assemble and disassemble the F-series tests. At TREAT, Bill Knapp as test coordinator was instrumental in the sucessful execution of all the F-series transients. Roger Conant assisted Bill Knapp. Gerry Larsen at TREAT worked on the reactor power control system. In addition, Gerry provided the experimenters with a first look at the F1 and F2 test data by digitizing the test data in the evening following each test. The entire operation staff at TREAT is acknowledged for their efforts.

Bill Kettman cut up the test capsule after the F2 test in the MSD alpha-gamma hot cell. Joe Florek prepared the F2 metallographic specimens.